Article

Cell Stem Cell

ASCL1 Reorganizes Chromatin to Direct Neuronal Fate and Suppress Tumorigenicity of Glioblastoma Stem Cells

Graphical Abstract

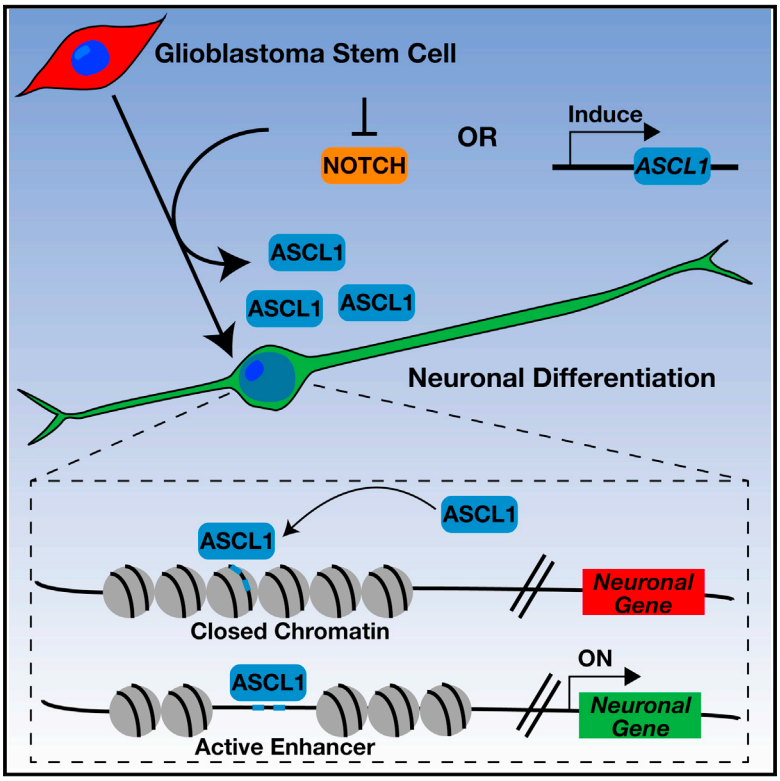

Highlights

- GSCs can be classified into two subgroups based on ASCL1 expression
- ASCL1 is required for GSCs to undergo neuronal lineage differentiation
- ASCL1^{hi} GSCs are responsive to Notch pathway inhibitors
- ASCL1 binds closed chromatin to activate target genes that drive neuronal fate

Authors

Nicole I. Park, Paul Guilhamon, Kinjal Desai, ..., Xi Huang, Mathieu Lupien, Peter B. Dirks

Correspondence

peter.dirks@sickkids.ca

In Brief

Glioblastoma is characterized by a block in cellular differentiation. Park et al. identify a subset of glioblastoma stem cells (GSCs) that express high levels of the proneural transcription factor ASCL1 and differentiate in response to Notch inhibition, effectively abrogating their stemness properties and tumorigenic potential.

Park et al., 2017, Cell Stem Cell *21*, 1–16
August 3, 2017 © 2017 Elsevier Inc.
http://dx.doi.org/10.1016/j.stem.2017.06.004

CellPress

Please cite this article in press as: Park et al., ASCL1 Reorganizes Chromatin to Direct Neuronal Fate and Suppress Tumorigenicity of Glioblastoma Stem Cells, Cell Stem Cell (2017), http://dx.doi.org/10.1016/j.stem.2017.06.004

Cell Stem Cell
Article

CellPress

ASCL1 Reorganizes Chromatin to Direct Neuronal Fate and Suppress Tumorigenicity of Glioblastoma Stem Cells

Nicole I. Park,[1,2] Paul Guilhamon,[3] Kinjal Desai,[1] Rochelle F. McAdam,[1,2] Ellen Langille,[2] Madlen O'Connor,[1] Xiaoyang Lan,[1,2] Heather Whetstone,[1] Fiona J. Coutinho,[1,2] Robert J. Vanner,[1,2] Erick Ling,[1,4] Panagiotis Prinos,[5] Lilian Lee,[1] Hayden Selvadurai,[1] Gurnit Atwal,[2] Michelle Kushida,[1] Ian D. Clarke,[1,6] Veronique Voisin,[7] Michael D. Cusimano,[8,9] Mark Bernstein,[8,10] Sunit Das,[8,9] Gary Bader,[2,7] Cheryl H. Arrowsmith,[3,5] Stephane Angers,[11] Xi Huang,[1,2] Mathieu Lupien,[3,12,13] and Peter B. Dirks[1,2,4,8,14,*]

[1]Developmental and Stem Cell Biology Program and Arthur and Sonia Labatt Brain Tumor Research Centre, The Hospital for Sick Children, Toronto, ON M5G 0A4, Canada
[2]Department of Molecular Genetics, University of Toronto, Toronto, ON M5S 1A8, Canada
[3]Princess Margaret Cancer Centre, University Health Network, Toronto, ON M5G 1L7, Canada
[4]Department of Laboratory Medicine and Pathobiology, University of Toronto, Toronto, ON M5S 1A8, Canada
[5]Structural Genomics Consortium, University of Toronto, Toronto, ON M5G 1L7, Canada
[6]OCAD University, Toronto, ON M5T 1W1, Canada
[7]The Donnelly Centre, University of Toronto, Toronto, ON M5S 3E1, Canada
[8]Division of Neurosurgery, University of Toronto, Toronto, ON M5S 1A8, Canada
[9]St. Michael's Hospital, Toronto, ON M5B 1W8, Canada
[10]Toronto Western Hospital, Toronto, ON M5T 2S8, Canada
[11]Leslie Dan Faculty of Pharmacy, University of Toronto, Toronto, ON M5S 3M2, Canada
[12]Department of Medical Biophysics, University of Toronto, Toronto, ON M5S 1A8, Canada
[13]Ontario Institute for Cancer Research, Toronto, ON M5G 0A3, Canada
[14]Lead Contact
*Correspondence: peter.dirks@sickkids.ca
http://dx.doi.org/10.1016/j.stem.2017.06.004

SUMMARY

Glioblastomas exhibit a hierarchical cellular organization, suggesting that they are driven by neoplastic stem cells that retain partial yet abnormal differentiation potential. Here, we show that a large subset of patient-derived glioblastoma stem cells (GSCs) express high levels of Achaete-scute homolog 1 (ASCL1), a proneural transcription factor involved in normal neurogenesis. ASCL1^{hi} GSCs exhibit a latent capacity for terminal neuronal differentiation in response to inhibition of Notch signaling, whereas ASCL1^{lo} GSCs do not. Increasing ASCL1 levels in ASCL1^{lo} GSCs restores neuronal lineage potential, promotes terminal differentiation, and attenuates tumorigenicity. ASCL1 mediates these effects by functioning as a pioneer factor at closed chromatin, opening new sites to activate a neurogenic gene expression program. Directing GSCs toward terminal differentiation may provide therapeutic applications for a subset of GBM patients and strongly supports efforts to restore differentiation potential in GBM and other cancers.

INTRODUCTION

Glioblastoma (GBM) is refractory to conventional therapies, and recent molecularly targeted approaches have not met desired expectations for improvements in survival (Carlsson et al., 2014; von Neubeck et al., 2015). Patient treatment failures, in part, can be explained by the high degree of molecular and functional heterogeneity between patient tumors and within the individual tumors themselves (Brennan et al., 2013; Meyer et al., 2015; Patel et al., 2014). So far, molecular stratification of GBMs has not led to the development of successful patient-specific therapies.

GBM and lower grade gliomas are organized as a hierarchy containing a subpopulation of cells that phenotypically and functionally resemble neural precursor cells (Singh et al., 2004; Tirosh et al., 2016). Functionally defined as glioblastoma stem cells (GSCs), these cells are enriched for tumor propagating potential and drive long-term disease progression in vivo (Chen et al., 2012; Gallo et al., 2015). As neural stem cells (NSCs) give rise to neuronal and glial progeny, associated with loss of self-renewal ability, promoting GSC differentiation may be a strategy to limit tumorigenic capacity by shifting the fate of cells to a mature post mitotic state. Indeed, bone morphogenetic protein (BMP) treatment promotes astrocytic differentiation of GBM cells and reduces tumorigenicity (Lee et al., 2008; Piccirillo et al., 2006) yet, astrocytes are prone to cell-cycle re-entry (Bardehle et al., 2013; Carén et al., 2015; Magnusson et al., 2014). Neurons represent terminally differentiated cell types with evidence for transformation-resistance in multiple models of GBM (Alcantara Llaguno et al., 2009, 2015; Friedmann-Morvinski et al., 2012). Therefore, directed specification of GSCs toward the neuronal lineage may be an effective strategy to limit tumorigenic potential.

The Notch pathway maintains NSC maintenance and inhibits neuronal differentiation by repressing the expression of

proneural transcription factors (TF) (Castella et al., 1999; Imayoshi et al., 2013; Kageyama et al., 2005). This repression includes Achaete-scute homolog 1 (ASCL1), an evolutionarily conserved basic-helix-loop-helix (bHLH) TF that is both necessary and sufficient for the generation of new neurons (Bertrand et al., 2002; Kim et al., 2011; Wilkinson et al., 2013). Enforced *ASCL1* expression in neural precursor cells or in a somatic non-neural cell context induces cell-cycle exit and full neuronal specification and differentiation (Berninger et al., 2007; Chanda et al., 2014; Pang et al., 2011).

In this study, we interrogated the differentiation potential of primary GSC cultures derived from patient samples and observed that only a subset retains neurogenic potential. We identified ASCL1 as critical for governing neuronal differentiation downstream of Notch pathway inhibition and determined ASCL1 directly regulates a program that promotes advanced neuronal fate and loss of self-renewal. Directed fate conversion by ASCL1 alone in GSCs reorganizes chromatin and initiates a neurogenic program that is tumorigenesis-resistant and suggests that directed neuronal lineage specification deserves further exploration in the clinic.

RESULTS

ASCL1 Expression Defines a Subgroup of Differentiation-Competent GBM

We found a binary pattern of *ASCL1* expression across 35 early passage primary GBM-derived GSC cultures by microarray analysis with 54% of cultures expressing relatively higher levels of *ASCL1*, hereafter referred to as ASCL1^{hi} (n = 19; mean Log2 = 11.49 ± 1.02), compared to ASCL1^{lo} GSC cultures (n = 16; mean Log2 = 6.19 ± 0.72; $p < 0.0001$) (Figure 1A). We validated differential *ASCL1* expression across 12 GSC cultures by qPCR (Figure S1A) and primary tissues by microarray analysis from The Cancer Genome Atlas and French Database (Gravendeel et al., 2009). Interestingly, the ASCL1^{hi} subgroup is associated with better overall survival in gliomas independent of *IDH1* status (Figure 1B). Overall survival in GBM patients alone (Figure S1B) and *IDH1* wild-type GBM patients (Figure S1C) are associated with a marginal but not statistical increase in survival.

We next performed gene set enrichment analysis (GSEA) comparing ASCL1^{hi} and ASCL1^{lo} GSC cultures using gene sets from the KEGG, REACTOME, Gene Ontology, and TCGA databases. The ASCL1^{hi} subgroup associated with Notch signaling (NES = 1.71; p = 0.02), neurogenesis (NES = 1.43; p = 0.02), and the proneural GBM subtype (NES = 1.76; p value = 0.01) (Figure 1C). Interestingly, 4 out of the top 20 genes that positively correlate with *ASCL1* expression based on the TCGA database includes Notch ligands *DLL1/3* and downstream targets *HES5/6* (Table S1). The ASCL1^{lo} subgroup associated with anti-apoptosis (NES = −1.45; p = 0.04), Hippo signaling (NES = −1.689; $p < 0.01$), and the mesenchymal GBM subtype (NES = −1.82; p value = 0.006; Figure 1C).

The Notch pathway inhibits neuronal differentiation of NSCs by negatively regulating *ASCL1* expression during neurogenesis (Kageyama et al., 2005). To interrogate whether this association between Notch signaling and *ASCL1* is conserved in GSC cultures, we perturbed Notch signaling with gamma-secretase inhibitors (GSIs), which block the final cleavage of the Notch receptor. ASCL1^{hi} (n = 3) and ASCL1^{lo} (n = 3) cultures were treated with 5 μM of GSI for 14 days and assessed for neuronal differentiation by immunocytochemistry. We observed a 6-fold increase in number of cells expressing neuronal tubulin beta 3 class III (TUBB3) in ASCL1^{hi} cultures (Figures 1D, 1E, S1D, and S1E) and no change in glial fibrillary acidic protein (GFAP) expression, indicating no concomitant astrocytic differentiation. None of the ASCL1^{lo} cultures displayed an increase in GFAP or TUBB3 in response to GSI. qPCR analysis also revealed an increase of *ASCL1* levels in ASCL1^{hi} GSCs after treatment with two independent GSIs, a finding that was not observed in ASCL1^{lo} GSCs (Figure 1F).

We further subjected ASCL1^{hi} and ASCL1^{lo} cultures to the growth factor withdrawal assay that is less specific in directing differentiation to a particular lineage. We compared GSC cultures that exhibited poor differentiation potential as we noted before (Pollard et al., 2009) with human-fetal neural stem (HFNS) cultures that are fully differentiation-competent. Exon microarray analysis revealed *ASCL1* was downregulated in poor-differentiating cultures under differentiation conditions (Figure 1G). By contrast, ASCL1^{hi} GSC and HFNS cultures displayed a consistent increase in *ASCL1* levels during differentiation (Figure 1H). There was a corresponding increase in TUBB3^{+} cells in ASCL1^{hi} GSCs, as assessed by immunocytochemistry (Figures S1F and S1G). TUBB3 expression remained unchanged in ASCL1^{lo} GSCs consistent with a blocked neuronal differentiation phenotype.

To determine whether lineage commitment results in reduced self-renewing ability, we plated cells in a limiting dilution analysis (LDA) and determined the frequency of clonal sphere-forming cells (SFCs). GSI treatment of ASCL1^{hi} GSCs exhibited a 10-fold decrease in SFCs ($p = 4.59 \times 10^{-7}$), while GSI treatment of ASCL1^{lo} GSCs had no effect on sphere-forming ability (p = 0.487; Figure 1I). To ensure these findings were not exclusive to cells adapted to serum-free culture, we examined primary GBM cells from freshly dissociated patient tumors (n = 4 primary GBMs). Half of the primary GBMs showed significant reductions in self-renewing frequency in response to GSI, whereas the remainder were unaffected (Figures 1J, 1K, S1H, and S1I). Critically, we confirmed that GSI responsive primary cultures had higher levels of *ASCL1* compared to those that failed to respond to GSI treatment (Figure S1A). To measure whether GSI-treated cells were able to revert back to a self-renewing state, spheres from the primary LDA were dissociated and re-plated in the absence of GSI in a secondary LDA. The ability to self-renew remained significantly abrogated in GSI-responsive GBM passage zero cells, demonstrating that this effect is irreversible (Figure 1L). Primary spheres that formed in the presence of GSI were able to form secondary spheres indicating continued resistance (Figure S1J). These data demonstrate a functional link between ASCL1 and the responsiveness to GSI treatment in both fresh primary and early passage cultures of GBM.

To confirm that GSI specifically inhibited Notch signaling, the effects on downstream components of the Notch pathway were measured. Cleaved Notch protein (NICD) was lost after 48 hr of GSI treatment compared to vehicle-treated GSCs (Figure S1K). Introduction of a dominant-negative construct of the Notch signaling transcriptional co-activator mastermind-like, DN-MAML (Weng et al., 2003) paralleled the effects of GSI

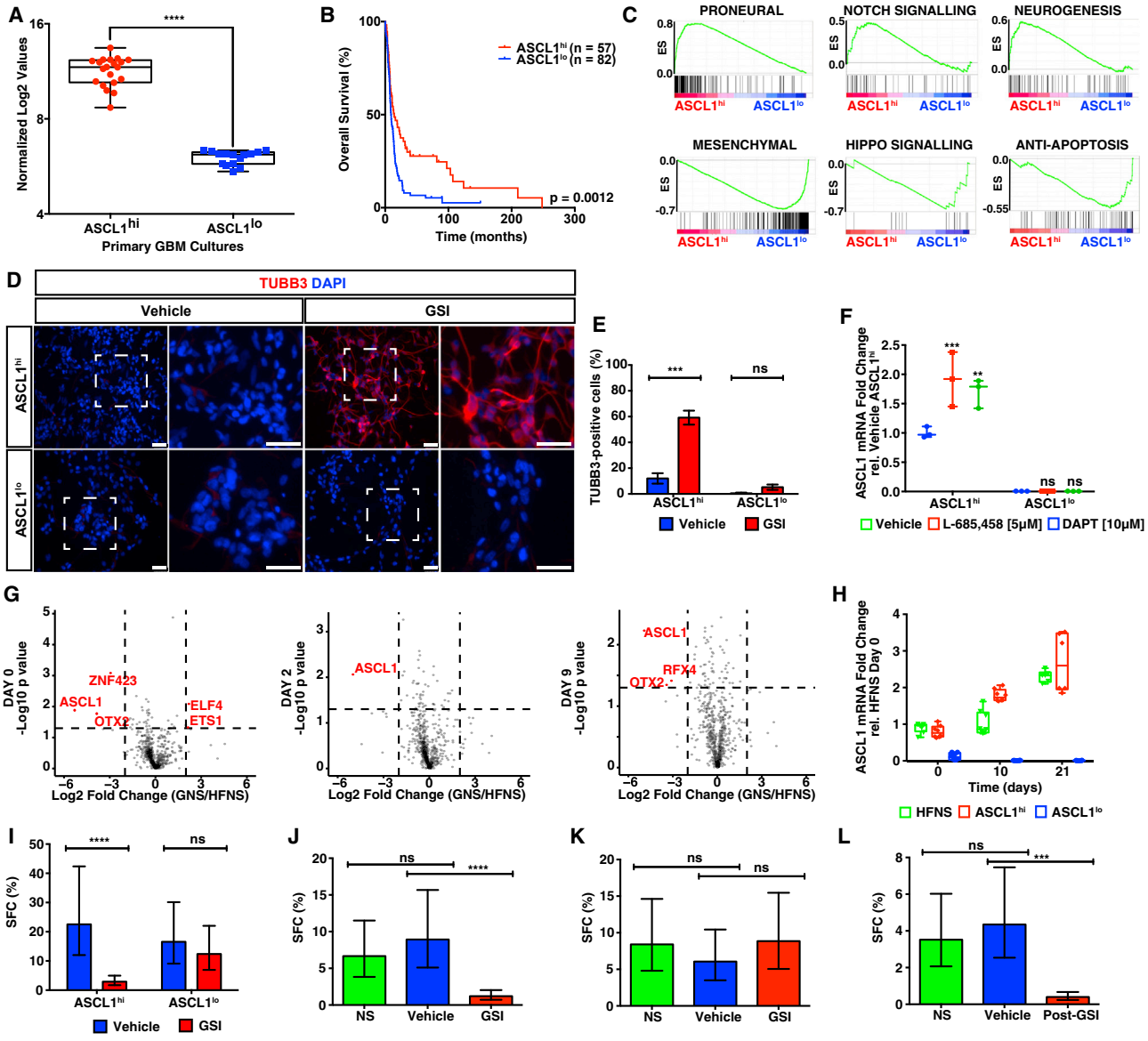

Figure 1. Characterization of ASCL1 in Primary GBM and GSC Cultures

(A) Box-and-whisker plots of microarray analysis of *ASCL1* expression in primary GSC cultures.

(B) Kaplan-Meier analysis relating ASCL1 expression with glioma patient survival.

(C) GSEA enrichment results of ASCL1^{hi} and ASCL1^{lo} GSC culture subgroups. ES, enrichment score.

(D) Immunocytochemical staining of TUBB3 of ASCL1^{hi} and ASCL1^{lo} GSCs treated with vehicle or GSI. Nuclei were stained by DAPI. Highlighted regions (white boxes) are shown at higher magnification on the right. DAPI, 4,6-diamidino-2-phenylindole. Scale bar, 50 μm.

(E) Quantification of TUBB3^{+} cells of ASCL1^{hi} ($p = 0.0013$) and ASCL1^{lo} ($p = 0.1502$) GSCs ($n = 3$ individual tumors each) treated with vehicle or GSI. Error bars, mean ± SEM.

(F) qPCR analysis of *ASCL1* mRNA levels of ASCL1^{hi} (GliNS1) and ASCL1^{lo} (G377NS) GSCs treated with vehicle, L-685,458, or DAPT (two-way ANOVA and Bonferroni post hoc tests; $^{**}p < 0.01$, $^{***}p < 0.001$). DAPT, N-[N-(3,5-difluorophenacetyl)-L-alanyl]-S-phenylglycine t-butyl ester. Error bars, median ± SD.

(G) Volcano plots of differentially expressed TFs (log2 fold change > ± 2; $p < 0.05$; red) between GSC and HFNS cultures at days 0, 2, and 9 under differentiation conditions.

(H) qPCR analysis of *ASCL1* mRNA levels of ASCL1^{hi} and ASCL1^{lo} GSCs ($n = 2$ individual tumors) under differentiation conditions. Error bars, median ± SD.

(I) In vitro LDA of ASCL1^{hi} (G362NS) and ASCL1^{lo} (G377NS) GSCs treated with vehicle or GSI. Error bars, estimated frequency ±95% confidence interval (CI).

(J) In vitro LDA of freshly dissociated GBM cells (GBM754) under NS conditions, or treated with vehicle ($p = 0.448$) or GSI ($p = 1.09 \times 10^{-6}$). Error bars, estimated frequency ±95% CI.

(K) In vitro LDA of freshly dissociated GBM cells (GBM753) under NS conditions, or treated with vehicle ($p = 0.377$) or GSI ($p = 0.321$). Error bars, estimated frequency ± 95% CI.

(L) Secondary in vitro LDA of GBM754 re-plated under NS conditions ($p_{DMSO} = 0.553$; $p_{GSI} = 1.47 \times 10^{-10}$). Error bars, estimated frequency ± 95% CI.

See also Figure S1 and Table S1.

resulting in downregulation of *HES1* and *HES5* levels and increase in *ASCL1* levels (Figure S1L). Knock out of *HES1* by CRISPR/Cas9 also resulted in increased *ASCL1* expression (Figure S1M), further demonstrating that active Notch signaling negatively regulates *ASCL1*. Importantly, the effect of GSI on Notch target genes was rescued upon overexpression of NICD (Figure S1N). NICD overexpression also blocked the differentiation phenotype observed after GSI treatment, assessed by staining of TUBB3 in addition to the stem cell markers Nestin and SOX2 (Figures S1O and S1P). The increase of neuronal marker expression in response to GSI treatment was coupled with a reduction in proliferation, a result also confirmed by transfection of DN-MAML (Figure S1Q).

Thus, *ASCL1* expression defines two distinct molecular subgroups of GBM and corresponding GSC cultures with a clear difference in capacity for neuronal differentiation. Our data indicate that GSI specifically impinges on Notch signaling, upregulates *ASCL1* expression, and promotes neuronal differentiation and loss of self-renewal in the subset of ASCL1^{hi} GSC cultures.

ASCL1 Is Required for GSI-Mediated Neuronal Differentiation

We next queried whether ASCL1 was required for GSCs to respond to GSI. We repressed ASCL1 function using a dominant-negative approach (DN-ASCL1) (Castro et al., 2006, 2011) resulting in ~80% reduction in ASCL1 reporter activity (Figures S2A and S2B). Transfections of DN-ASCL1 or non-targeting vector in ASCL1^{hi} cultures (n = 3) was followed by GSI treatment. Transfection of ASCL1^{lo} (n = 2) cultures served as negative controls for all functional experiments.

We observed abrogated neuronal differentiation in DN-ASCL1 transfected ASCL1^{hi} cultures treated with GSI, similar to the responses observed of ASCL1^{lo} cultures (Figures 2A, 2B, and S2C–S2G). Control ASCL1^{hi} GSCs exhibited an increase in TUBB3^{+} cells (88% ± 2.25%), with no evidence of astrocytic differentiation (Figures 2A–2C and S2C–S2E). A concomitant decrease in proliferation of control ASCL1^{hi} GSCs was observed by a 2-fold increase in population doubling time (Figures 2D and S2H). Confirming the requirement for ASCL1 to mediate the effects of GSI, transfection of DN-ASCL1 resulted in no effect on proliferation. We also observed no changes to proliferation of ASCL1^{hi} or ASCL1^{lo} cultures when ASCL1 was repressed (Figure S2I). Thus, in the absence of an appropriate differentiation signal, ASCL1 is not able to overcome proliferation of GBM cells that are in a precursor state, nor does it promote their proliferation. Consistent with a loss of self-renewal ability, GSI effects on control transfected cultures was abolished in the DN-ASCL1 setting and the fraction of SFCs remained unchanged (Figures 2E, 2F, and S2J–S2M).

We next investigated whether the relationship between ASCL1 and GSI treatment effects seen in culture was conserved in vivo. Control or DN-ASCL1 transfected ASCL1^{hi} GSCs were treated with GSI before orthotopic xenotransplantation. GSI treatment extended tumor latency in the control group and median survival increased from 22 to 34 days (p = 0.0008; Figure 2G). Survival of the DN-ASCL1 group remained unchanged between treatment conditions confirming that survival increase is dependent on the action of ASCL1. There was no change in overall survival between vehicle treatment groups, further demonstrating that loss of ASCL1 does not cause a reduction in proliferation and tumorigenicity.

To more thoroughly probe the functional requirement of ASCL1 and mitigate potential off-target effects of a dominant-negative approach, we generated *ASCL1* genetic knockout cultures using the CRISPR/Cas9 system. Transfection of two gRNAs targeting *ASCL1* resulted in an ~360 bp deletion, as confirmed by sequencing (Figures S2N and S2O). This corresponds to a 50.6% deletion that includes the entire bHLH domain. Single cell-derived clonal cultures harboring null and wild-type *ASCL1* were denoted as ASCL1^{KO} and ASCL1^{WT}, respectively. Loss of *ASCL1* mRNA and protein were confirmed by qPCR and western blot analysis, respectively (Figures S2P and S2Q).

Consistent with our findings above, we found an increase in TUBB3^{+} cells after GSI treatment of ASCL1^{WT} GSCs, while this effect was abrogated in ASCL1^{KO} GSCs (Figure 2H), and these cells failed to increase TUBB3^{+} cells under growth-factor withdrawal conditions (Figure S2R). Thus, ASCL1 mediates neuronal fate responses outside the context of Notch signaling. We also confirmed that GSI-mediated reduction on self-renewal of GSCs is dependent on ASCL1 by performing LDAs on independent ASCL1^{KO} clonal cultures (Figure 2I).

Using immunofluorescence, we could detect ASCL1 in 35.68% ± 6.73% of the ASCL1^{WT} culture that increased to 72.27% ± 3.55% upon treatment with GSI (p = 0.008) (Figures 2J and 2K). Co-staining with the proliferation marker, Ki67, revealed a decrease of cycling ASCL1^{+} cells from 35.59% ± 0.84% to 19.94% ± 3.98% (p = 0.0002) (Figure 2L) while there was no change in the frequency of Ki67^{+} cells in the ASCL1 negative fraction between treatment conditions. Thus, GSI treatment results in an increase in ASCL1^{+} cells and selectively reduces proliferation of this cell fraction.

ASCL1 Alone Is Sufficient to Induce Neuronal Differentiation of GSCs

We next sought to restore ASCL1 expression to ASCL1^{lo} and ASCL1^{KO} GSC cultures. Cells were stably transduced with a tetON-ASCL1 cassette such that *ASCL1* is expressed in the presence of doxycycline (DOX) (Figure 3A). qPCR and immunofluorescence confirmed *ASCL1* mRNA and protein levels were induced (Figures 3B and 3C).

Forced expression of *ASCL1* resulted in a significant increase in TUBB3^{+} cells displaying mature, elongated, and extended neurites reminiscent of maturing neurons (Figures 3C and 3D; Movie S1). Immunofluorescence revealed ASCL1 promoted MAP2, NEUN, VGLUT1, and GABA expression in both ASCL1^{KO} and ASCL1^{lo} cultures (Figures S3A–S3D), consistent with a mature neuronal fate and a lack of astrocytic differentiation by S100β expression (Figure S3A). Thus, expression of ASCL1 in GSCs promoted a pan-neuronal fate, producing mature neuronal cell types of both glutamatergic and GABAergic identity consistent with induced neuronal reprogramming studies (Pang et al., 2011; Vierbuchen et al., 2010).

We further investigated whether neuronal differentiation by ASCL1 was accompanied by defects in proliferation and self-renewal. We measured proliferation by cell counting, live-cell imaging, and incorporation of the thymidine analog, 5-ethynyl-2′-deoxyuridine (EdU). We induced ASCL1 expression for 14 days then pulsed with EdU for 3 hr and quantified for co-labeling with

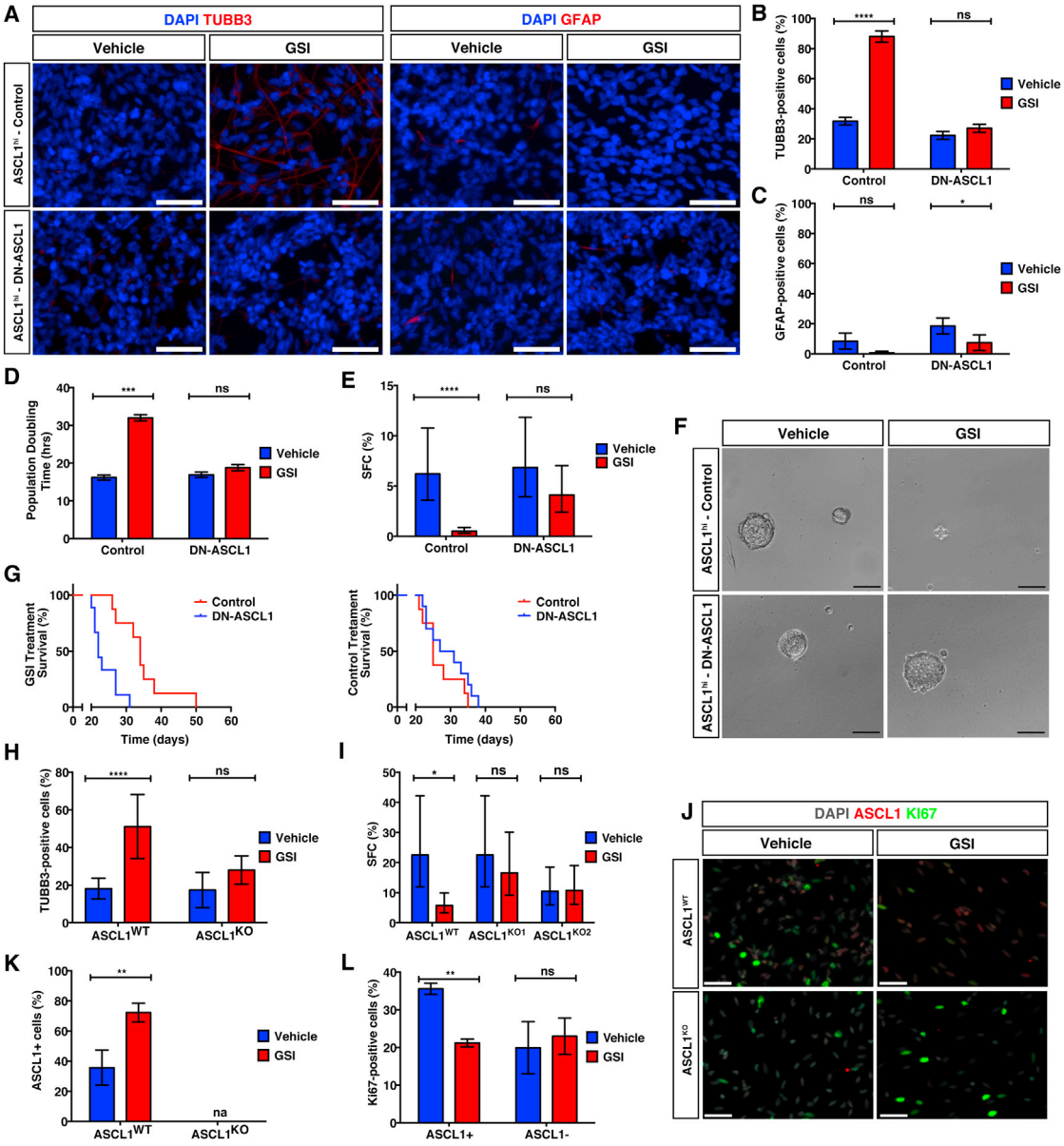

Figure 2. ASCL1 Function Is Required for Neuronal Fate Commitment

(A) Immunocytochemical staining of TUBB3 and GFAP in ASCL1^{hi} GSCs (GLINS1) transfected with control or DN-ASCL1 and treated with vehicle or GSI. Nuclei were stained by DAPI. Scale bar, 50 μm.

(B) Quantification of TUBB3^{+} cells of ASCL1^{hi} GSCs transfected with control ($p < 0.0001$) or DN-ASCL1 ($p = 0.1136$) treated with vehicle or GSI. Error bars, mean ± SEM.

(C) Quantification of GFAP+ cells of ASCL1^{hi} GSCs transfected with control ($p = 0.0617$) or DN-ASCL1 ($p = 0.01$) treated with vehicle or GSI. Error bars, mean ± SEM.

(D) Population doubling times of ASCL1^{hi} GSCs (G362NS) transfected with control ($p = 0.0008$) or DN-ASCL1 ($p = 0.4428$) treated with vehicle or GSI. Error bars, mean ± SEM.

(E) In vitro LDA of GSI-treated ASCL1^{hi} GSCs (G362NS) transfected with control ($p = 1.09 \times 10^{-6}$) or DN-ASCL1 ($p = 0.15$). Error bars, estimated frequency ±95% CI.

(F) Representative spheres of ASCL1^{hi} GSCs (G362NS) transfected with control vector or DN-ASCL1 construct treated with vehicle or GSI. Scale bar, 75 μm.

(G) Kaplan-Meier analysis of ex vivo GSI and vehicle-treated ASCL1^{hi} GSCs transfected with control or DN-ASCL1.

(H) Quantification of TUBB3^{+} cells of ASCL1^{WT} ($p < 0.0001$) and ASCL1^{KO} ($p = 0.1196$) GSCs treated with vehicle or GSI. Error bars, mean ± SEM.

(I) In vitro LDA of ASCL1^{WT} ($p = 0.0252$) or ASCL1^{KO} ($n = 2$; $p_{KO1} = 0.489$; $p_{KO2} = 0.781$) cultures treated with vehicle or GSI. Error bars, estimated frequency ±95% CI.

(J) Immunocytochemical staining of ASCL1 and Ki67 of ASCL1^{WT} and ASCL1^{KO} GSCs treated with vehicle or GSI. Nuclei were stained by DAPI. Scale bar, 50 μm.

(K) Quantification of ASCL1^{+} cells in ASCL1^{WT} and ASCL1^{KO} GSCs treated with vehicle or GSI. Error bars, mean ± SEM.

(L) Quantification of Ki67^{+} cells within the ASCL1^{+} and ASCL1^{-} population under vehicle or GSI conditions. Error bars, mean ± SEM.

See also Figure S2.

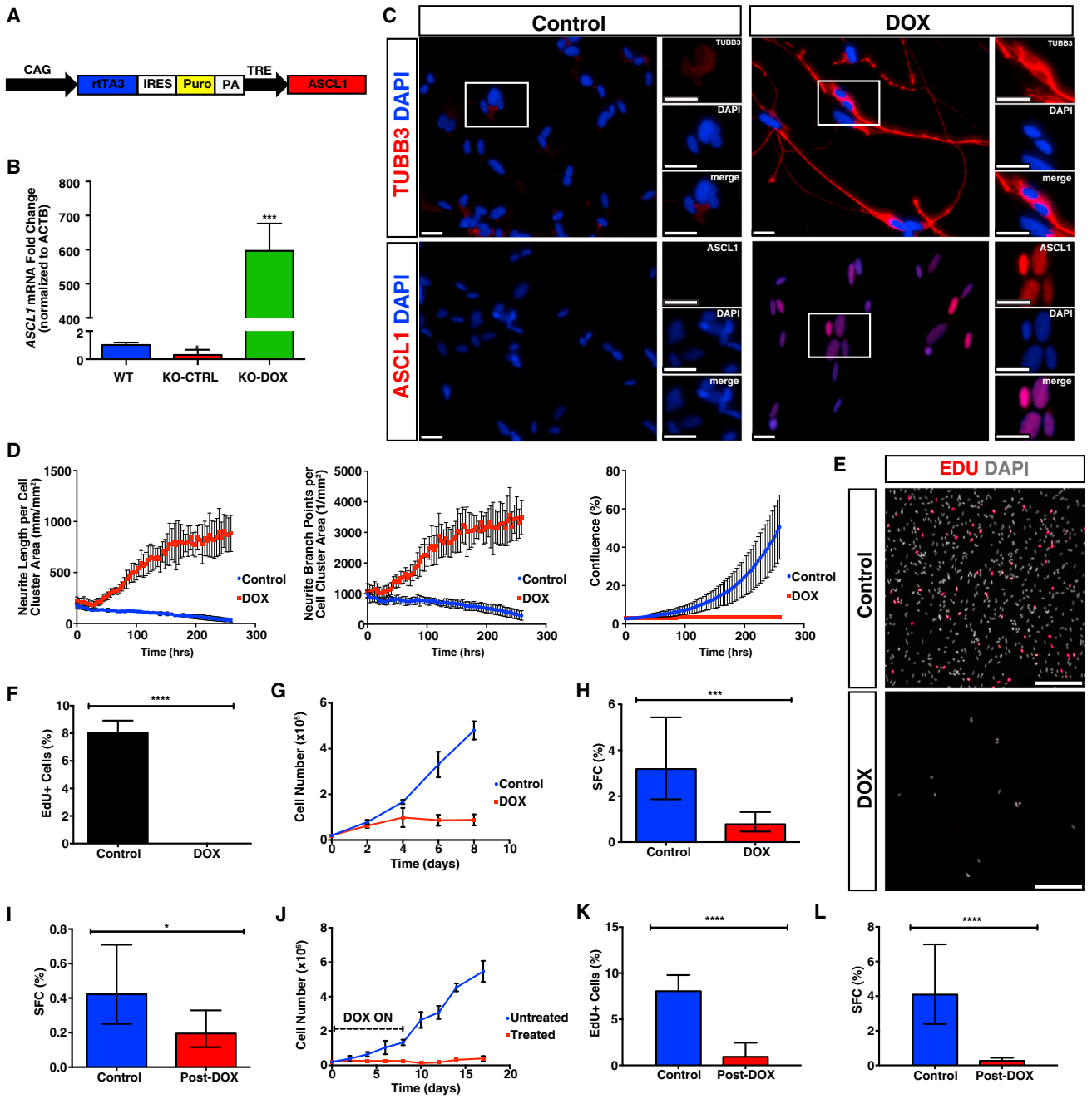

Figure 3. ASCL1 Alone Is Sufficient to Promote the Neuronal Fate of GSCs

(A) Diagram of Tet-ON-ASCL1 construct.

(B) qPCR analysis of *ASCL1* mRNA levels of ASCL1^{WT} and ASCL1^{KO} GSCs ($p = 0.0397$) treated with DOX ($p = 0.0008$). Error bars, mean ± SD.

(C) Immunocytochemical staining of TUBB3 and ASCL1 of ASCL1^{KO} GSCs induced with DOX. Nuclei were stained by DAPI. Scale bar, 50 μm.

(D) Quantification of neurite length, neurite branch points, and cell confluency of ASCL1^{KO} GSCs in the presence or absence of DOX. Error bars, mean ± SD.

(E) Immunocytochemical staining of EdU of ASCL1^{KO} GSCs induced with DOX. Nuclei were stained by DAPI. EdU, 5-ethynyl-2′-deoxyuridine. Scale bar, 250 μm.

(F) Quantification of EdU^{+} cells of ASCL1^{KO} GSCs induced with DOX ($p < 0.0001$). Error bars, mean ± SEM.

(G) Quantified cell numbers of ASCL1^{lo} GSCs during DOX treatment.

(H) In vitro LDA of ASCL1^{KO} GSCs induced with DOX ($p = 0.00013$). Error bars, estimated frequency ±95% CI.

(I) Secondary in vitro LDA of ASCL1^{KO} GSCs after DOX induction for 7 days ($p = 0.0409$). Error bars, estimated frequency ±95% CI.

(J) Quantified cell numbers of ASCL1^{KO} GSCs during and after DOX treatment.

(K) Quantification of EdU^{+} cells of ASCL1^{KO} GSCs 10 days after DOX treatment ($p = 0.0009$). Error bars, mean ± SEM.

(L) Secondary in vitro LDA of ASCL1^{KO} GSCs after DOX induction in adherent conditions ($p = 3.72 \times 10^{-12}$). Error bars, estimated frequency ±95% CI.

See also Figure S3 and Movie S1.

neuronal markers. The increase in mature neuronal cells, ~70% of cells positive for MAP2 or NEUN, were not dividing as measured by a lack of EdU label incorporation (Figures S3C and S3D). While 8.05% of control GSCs had incorporated label within a 3-hr period, inducing ASCL1 expression resulted in a complete loss of cycling cells (Figures 3E and 3F). After 10 days of induction, ASCL1^{lo} GSCs were unable to propagate the culture (Figure 3G). To determine whether the observed decreased in proliferation was simply due to cell death, we stained for cleaved caspase-3 and found no increase in apoptosis following 8 days of DOX treatment in comparison to control (Figures S3E and S3F). To measure self-renewal, we found a marked reduction (75.6%) in SFCs (Figure 3H). Upon re-plating in the absence of DOX, the loss of SFCs was sustained (Figure 3I). Similarly, after 8 days of DOX induction, ASCL1^{KO} cells failed to regenerate the culture even when in the presence of pro-proliferative growth factors for an additional 8 days (Figure 3J). Further, EdU labeling of cells 10 days after DOX removal confirmed a sustained lack of proliferation (Figure 3K).

To further demonstrate whether ASCL1-induced cells are able to revert back to a self-renewing state, we treated GSCs with DOX for 8 days and re-plated the cells in single-cell suspensions in the presence of growth factors. The ability to form spheres was markedly blocked, resulting in a 96-fold reduction in self-renewal potential, with only 0.06% of cells capable of initiating a colony (Figure 3L), despite the cells being cultured in pro-proliferative conditions. Thus, forced ASCL1 expression leads to overt neuronal differentiation with a loss of proliferative and self-renewing capacity. These data complement the functional effects of GSI treatment of ASCL1^{hi} GSCs and demonstrate that driving *ASCL1* expression in ASCL1^{lo} cells restores neuronal differentiation capacity.

ASCL1 Overexpression Attenuates GBM Progression In Vivo

We performed intracranial transplantations of ASCL1^{lo} GSCs transduced with inducible-ASCL1 (n = 16 mice). Half of the injected mice were fed with a DOX diet. Control ASCL1^{lo} GSCs engrafted large intracranial masses and showed areas of immunoreactivity for Ki67 with lack of TUBB3 staining (Figure 4A), consistent with failed differentiation. DOX-treated tumors by comparison, showed slower growth, with an increase in overall survival from 24 to 35 days ($p < 0.0001$) (Figure 4B). Tumors that eventually formed in the DOX-treated group were largely comprised of ASCL1-negative cells (Figures S4A and S4B), suggesting escape from ASCL1 expression. We next performed ex vivo DOX treatment prior to orthotopic transplantation that resulted in further increased survival with 50% of animals still alive at 157 days (Figure 4B). We determined whether increased survival from in vivo DOX induction was due to a decrease in number of clonogenic cells. We harvested endpoint tumors and plated primary xenograft cells in a sphere assay. We observed the mean fraction of SFCs decreased 23-fold from 0.69% ± 0.396% to 0.03% ± 0.004% ($p = 0.0003$) (Figure S4C) after induction of ASCL1 in vivo, therefore, resulting in a significantly reduced fraction of self-renewing cells in the residual lesions. Furthermore, serial dilutions of primary xenograft cells in a secondary transplantation assay revealed a 10-fold reduction in tumor-initiating cells from DOX-treated mice (Figure 4C). Together, our data demonstrate that enforced ASCL1 expression promotes the differentiation of GSCs in vivo and is accompanied by reduced tumor propagating potential.

We further investigated the role of ASCL1 in an in situ GBM model. We utilized *Drosophila melanogaster* and the Gal4/UAS system to specifically express commonly altered human GBM oncogenes (activated EGFR and PIK3CA) in fly glia cells. Constitutive active forms of EGFR (*dEGFR*$^{\lambda}$) and PIK3CA (*dp110*^{CAAX}) were expressed in Repo^{+} glial cells (*repo-Gal4 > dEGFR*$^{\lambda}$*; dp110*^{CAAX}), which resulted in fully penetrant GBM tumorigenesis in fly CNS due to massive glial overproliferation (Read et al., 2009). The *repo-Gal4* driver expresses both the oncogenes and mCherry that was used to quantify GBM tumor size. We combined this model with the UAS-driven fly *Achaete* (*ac*) or human *ASCL1* (Hsap/ASCL1), followed by staining for markers of proliferation, neuronal, and glial differentiation. Concurrent expression of either fly Achaete or human ASCL1 specifically in the fly GBM cells led to overall smaller CNS structures (Figures 4D, 4E, and S4D). There was an ~80% reduction in mCherry^{+} GBM tumor size due to Achaete expression ($p_{ac} < 0.0001$) and ~50% reduction due to human ASCL1 expression ($p_{ASCL1} = 0.0003$). Cyclin B expression confirmed a decrease in proliferation ($p_{ac} < 0.0006$) and a 2.5- to 4-fold increase in neuronal expression as measured by the expression of Elav, a marker for differentiated fly neurons ($p_{ac} < 0.0001$; $p_{ASCL1} < 0.0001$) (Figures 4F, 4G, and S4E). Strikingly, while cells in the control brains adopted either a glial or neuronal fate, we detected double positive Repo and Elav events in the GBM of *repo-Gal4 > dEGFR*$^{\lambda}$*; dp110*^{CAAX}*; ac* brains, demonstrating an in vivo switch of glial-to-neuronal fate due to Achaete function in the tumor cells (Figure 4H). On average, we observed 4.92 double-positive events per larvae in the Achaete group compared to 0.2 double-positive events in the control tumor model (Figure 4I). These data demonstrate the highly conserved role of proneural TFs in directing the fate of tumorigenic glial cells toward cell types resembling neuronal cells and consequently reducing tumor burden in a complementary in vivo GBM model system.

ASCL1 Upregulates a Neurogenic Program in GSCs

We sought to identify the downstream targets of ASCL1 that mediate neuronal differentiation of GSCs in response to GSI treatment. We performed RNA sequencing (RNA-seq) analysis of ASCL1^{KO} (n = 3) and ASCL1^{WT} cultures (n = 3) after treatment with GSI (Figure S5A). We identified 2,666 differentially expressed genes when ASCL1^{WT} cells were treated with GSI (Figure 5A). Conversely, ASCL1^{KO} cells displayed proportionately less change when treated with GSI (n = 815 genes), suggesting that GSI modulates additional molecular programs independent of neuronal induction in the absence of ASCL1. We performed GSEA and identified genes associated with terms such as neuronal fate commitment, negative regulation of glial differentiation, and chromatin acetylation that were upregulated in GSI-treated ASCL1^{WT} cells (Figure 5B; Table S2). In contrast, there is downregulation of these genes in GSI-treated ASCL1^{KO} cells, and instead, immune response and oxidative stress response terms were enriched (Figure S5B; Table S3). We confirmed *ASCL1* and neuronal genes (i.e., *TNR*, *MAP2*, *DLX2*, *DCX*) were exclusively upregulated in ASCL1^{WT} GSCs treated with GSI (Figures 5C and 5D).

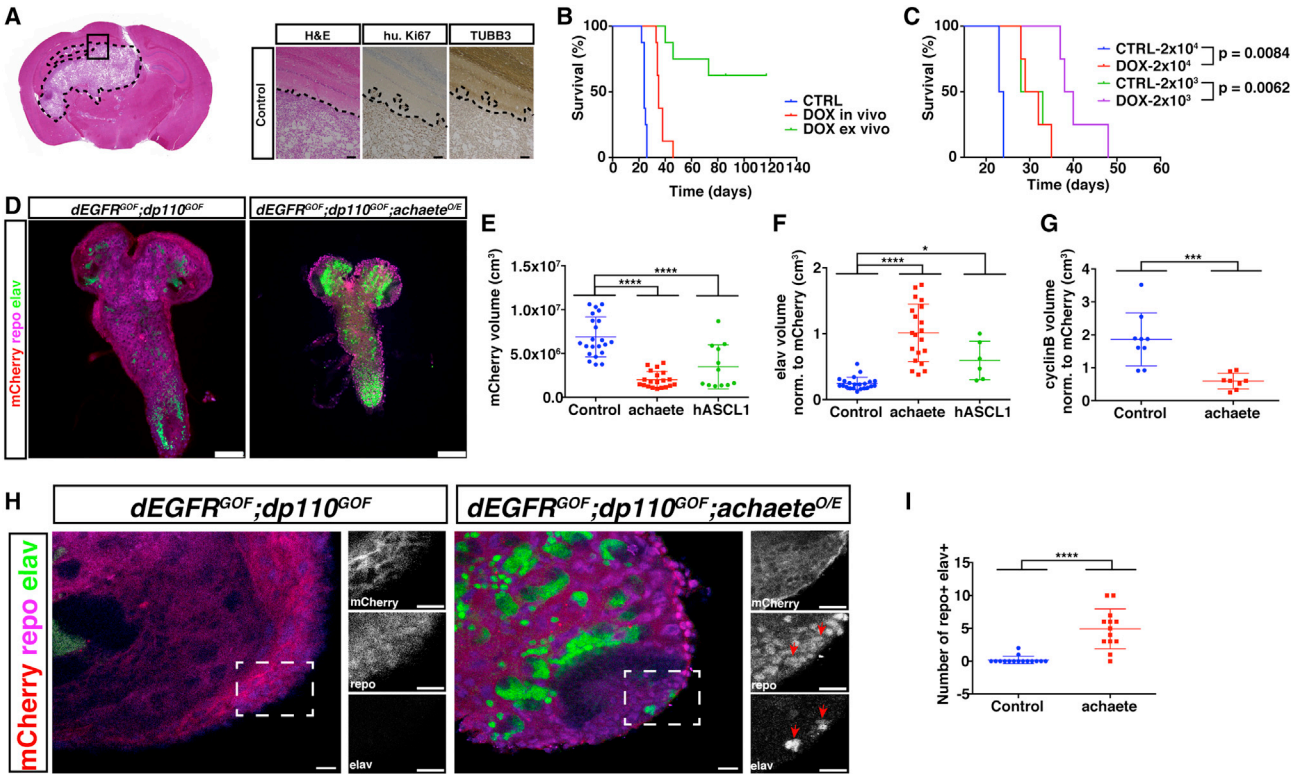

Figure 4. Enforced ASCL1 Expression Abrogates Tumorigenicity In Vivo

(A) H&E staining of a mouse brain injected with 20,000 ASCL1^{lo} GSCs shows an intracranial mass (dotted line), higher magnification (black inset) staining of human-specific Ki67 and TUBB3. Scale bar, 100 μm.

(B) Kaplan-Meier analysis of transplanted ASCL1^{lo} GSCs untreated or treated with DOX in vivo or ex vivo.

(C) Kaplan-Meier analysis of secondary transplantations of 20,000 cells and 2,000 cells after in vivo DOX treatment compared to control.

(D) Whole brain-ventral nerve cord complexes from late third instar larvae. In *repo* > *dEGFR*^{GOF};*dp110*^{GOF} larvae, both brain hemispheres and the VNC are enlarged relative to *repo* > *dEGFR*^{GOF};*dp110*^{GOF};*ac*$^{O/E}$. Scale bar, 100 μm.

(E) Quantification of tumor volume by mCherry in *ac*$^{O/E}$ (n = 20) and *ASCL1*$^{O/E}$ (n = 12) compared to control (n = 22). Error bars, mean ± SD.

(F) Quantification of Elav expression in *ac*$^{O/E}$ (n = 20) and hASCL1$^{O/E}$ (n = 6) and control (n = 22). Error bars, mean ± SD.

(G) Quantification of cyclin B expression in achaete$^{O/E}$ (n = 8) and control (n = 9). Error bars, mean ± SD.

(H) Co-expressing Elav and Repo cells (red arrows) in *ac*$^{O/E}$ brains. Scale bar, 12.5 μm.

(I) Overexpression of *ac* (n = 13) results in increased glial and neuronal co-expressing cells compared to control (n = 15; $p < 0.0001$). Error bars, mean ± SD.

See also Figure S4.

To validate ASCL1 targets, we performed RNA-seq of ASCL1^{KO} GSCs after *ASCL1* induction for 7 days. Nearly 90% of differentially expressed genes identified from GSI treatment of ASCL1^{WT} cells overlapped with differentially expressed genes when ASCL1^{KO} cells were induced to express *ASCL1*, consistent with a prominent ASCL1-dependent and Notch-dependent neuronal induction (Figure 5E). These genes included neuronal genes *TNR*, *ELAVL4*, and a potassium channel gene *KCNK3* (Figure 5F), while expression of NSC markers, *SOX2* and *NES*, were downregulated in *ASCL1*-induced cells (Figure S5C). These findings strongly support a neurogenic role of ASCL1 under GSI conditions and further nominate additional targets of ASCL1 in the neuronal differentiation of GSCs. Furthermore, 76 putative ASCL1 target genes were upregulated in the ASCL1^{hi} subgroup (Table S4), many of which include genes that classify the proneural subtype. As our initial characterization support that ASCL1^{hi} subgroup is associated with the proneural subtype (Figure 1C), we observed that loss of *ASCL1* was sufficient to alter subtype identities from proneural (NES = −1.90; false discovery rate [FDR] < 5%) to mesenchymal (NES = 1.55; FDR < 5%) (Figures S5D and S5E) suggesting further that ASCL1 has a master-regulatory neurogenic role in GBM.

ASCL1 Binds to Closed Chromatin in Promoter and Enhancer Regions of Neuronal Target Genes

To determine whether ASCL1 directly occupied the promoter regions of neuronal genes identified from our RNA-seq analysis, we performed ASCL1 chromatin immunoprecipitation sequencing (ChIP-seq) of ASCL1^{KO} GSCs after 18 hr of DOX induction. Untreated ASCL1^{KO} cells served as a negative control for ChIP with the ASCL1 antibody. We identified 3,341 regions bound by ASCL1 that corresponded to mostly intronic (48%) and intergenic (36%) regions with 7.38% of peaks corresponding to exonic regions (Figure 6A). In comparison to the genomic background distribution of annotated regions, there was a 2.73 log2 enrichment of ASCL1 binding in exonic regions and a 2.4- and 1.84- log2 enrichment of ASCL1 binding in 5′UTR and promoter regions, respectively (Figures 6A and S6A). Motif enrichment analysis of

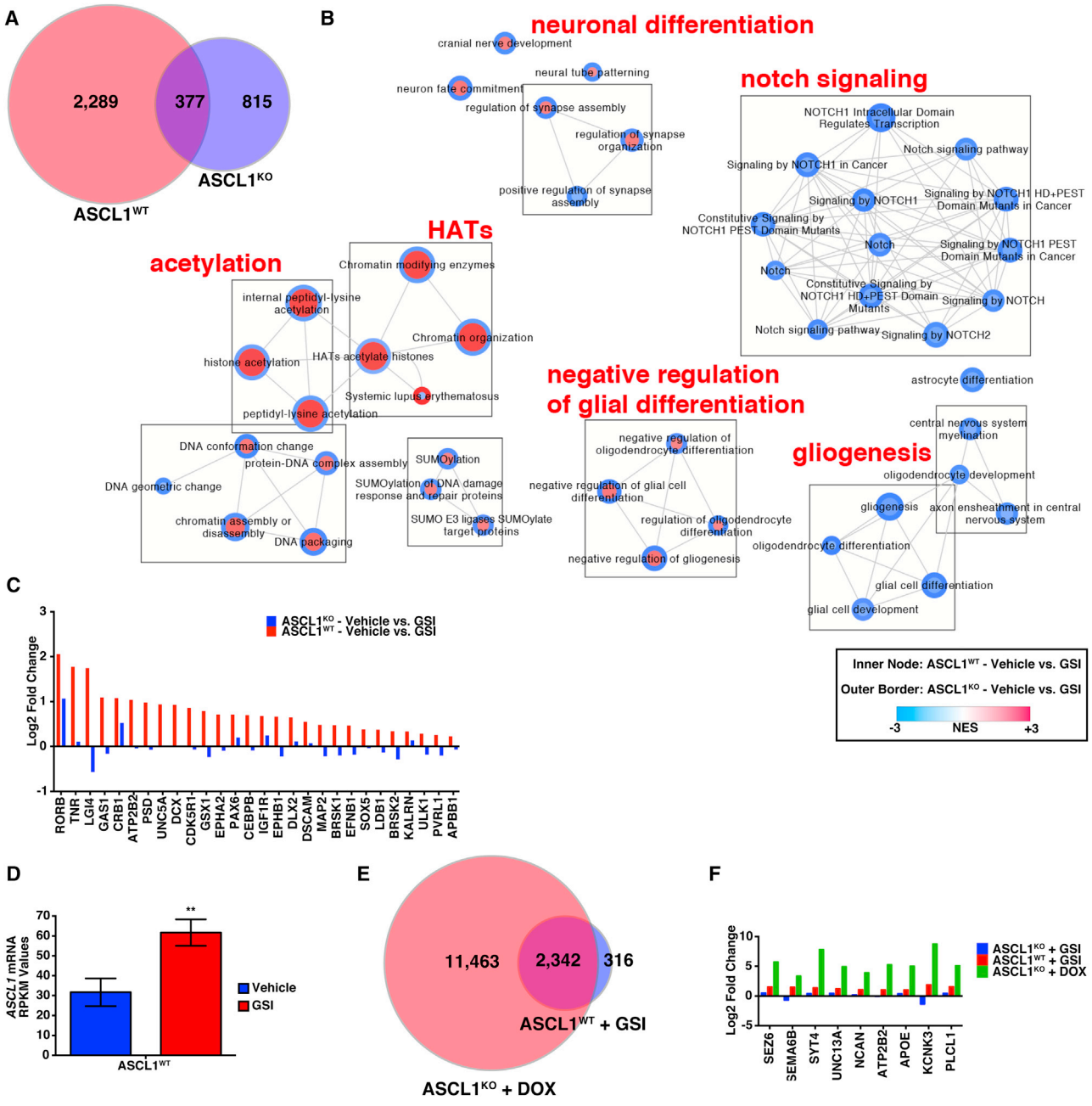

Figure 5. RNA-Seq Analysis Reveals ASCL1 Neuronal Target Genes in GBM

(A) Venn diagram displaying the number of differentially expressed genes (FDR < 5%) between ASCL1^{WT} GSCs treated with GSI and ASCL1^{KO} GSCs treated with GSI.

(B) Enrichment map of gene set terms enriched in GSI-treated ASCL1^{WT} and ASCL1^{KO} cells relative to vehicle treatment (FDR < 0.001).

(C) Neuronal differentiation genes are upregulated (FDR < 5%) in ASCL1^{WT} GSCs treated with GSI compared to ASCL1^{KO} GSCs.

(D) RNA-seq analysis of *ASCL1* in ASCL1^{WT} GSCs treated with vehicle or GSI (n = 3 biological replicates; p = 0.0056). Values are represented as reads per kilobase of transcript per million mapped reads (RPKM). Error bars, mean ± SEM.

(E) Venn diagram displaying the number of differentially expressed genes (FDR < 5%) between ASCL1^{WT} GSCs treated with GSI and ASCL1^{KO} GSCs induced with DOX.

(F) Neuronal differentiation and synaptic signaling genes are upregulated in ASCL1^{WT} GSCs treated with GSI and ASCL1^{KO} GSCs induced with DOX (FDR < 5%), compared to ASCL1^{KO} GSCs treated with GSI.

See also Figure S5 and Tables S2, S3, and S4.

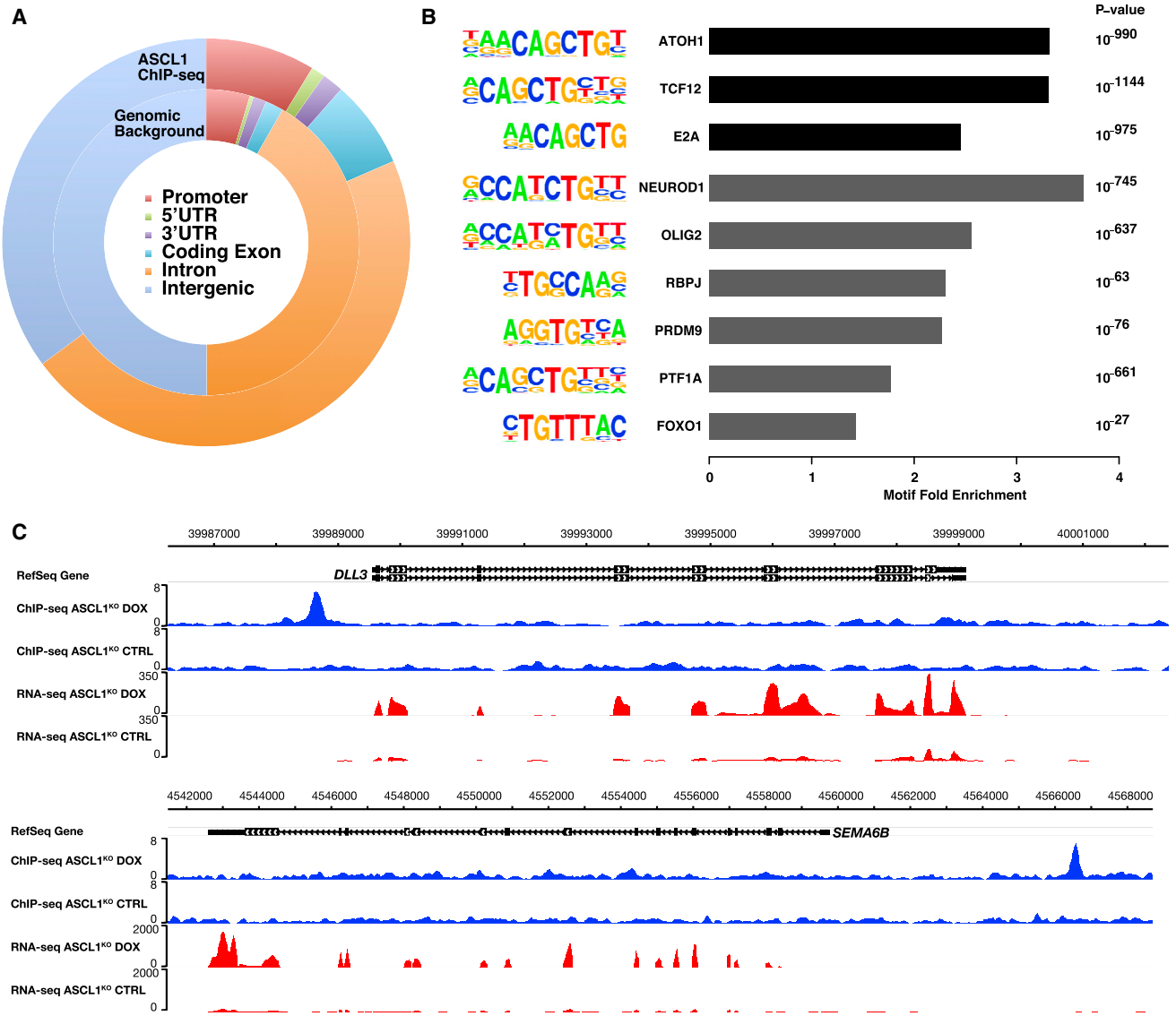

Figure 6. ASCL1 Binds to Promoter Regions of Neuronal Target Genes

(A) Doughnut charts displaying the genomic distribution ASCL1-binding sites compared to background.

(B) Motif analysis revealed factors that recognize the CAGCTG motif (black) and other potential co-factors (gray) were enriched in ASCL1-bound regions.

(C) Alignment data of ASCL1 ChIP-seq (blue) and RNA-seq (red) of ASCL1^{KO} GSCs treated with DOX near the *DLL3* and *SEMA6B* locus (black).

See also Figure S6 and Table S5.

ASCL1-bound regions revealed consensus sequences recognized by ASCL1 (CAGCTG) and other neurogenic factors (NEUROD1 and PTF1A) were enriched suggesting potential co-factors in regulating neuronal gene activation (Figure 6B). Enrichment of OLIG2, RBPJ, and FOXO1 motifs also point to the potential role of these factors in restraining ASCL1-dependent neurogenesis in GSCs that has been previously identified in mouse NSCs (Castro et al., 2011; Webb et al., 2013).

Comparison with previous ASCL1 ChIP experiments performed in mouse neural precursors confirmed a common set of genes near ASCL1 binding sites (n = 160) (Figure S6B). We identified promoters of genes associated with ASCL1 binding sites if peaks occurred within 5 kb upstream and 1 kb downstream transcriptional start sites. We joined our ChIP-seq and RNA-seq data of *ASCL1*-induced GSCs that revealed 344 genes that are upregulated >1.5-fold (FDR < 5%) and associated with ASCL1 binding within promoter regions (Table S5). Visualization of ChIP-seq and RNA-seq reads located near downstream targets of ASCL1 (e.g., *DLL3*) as well as neuronal genes are displayed (Figures 6C, S6C, and S6D). *SEMA6B* encodes for a semaphorin gene involved in axon guidance. ASCL1 binds ~6 kb upstream *SEMA6B*, and mRNA levels of *SEMA6B* are increased upon overexpression of *ASCL1* in ASCL1^{KO} cells. The regulation by ASCL1 on other neuronal genes, like *MYT1* and other well-characterized ASCL1 target genes like *DLL1*, are displayed. We also observed ASCL1 occupancy on many ion channel

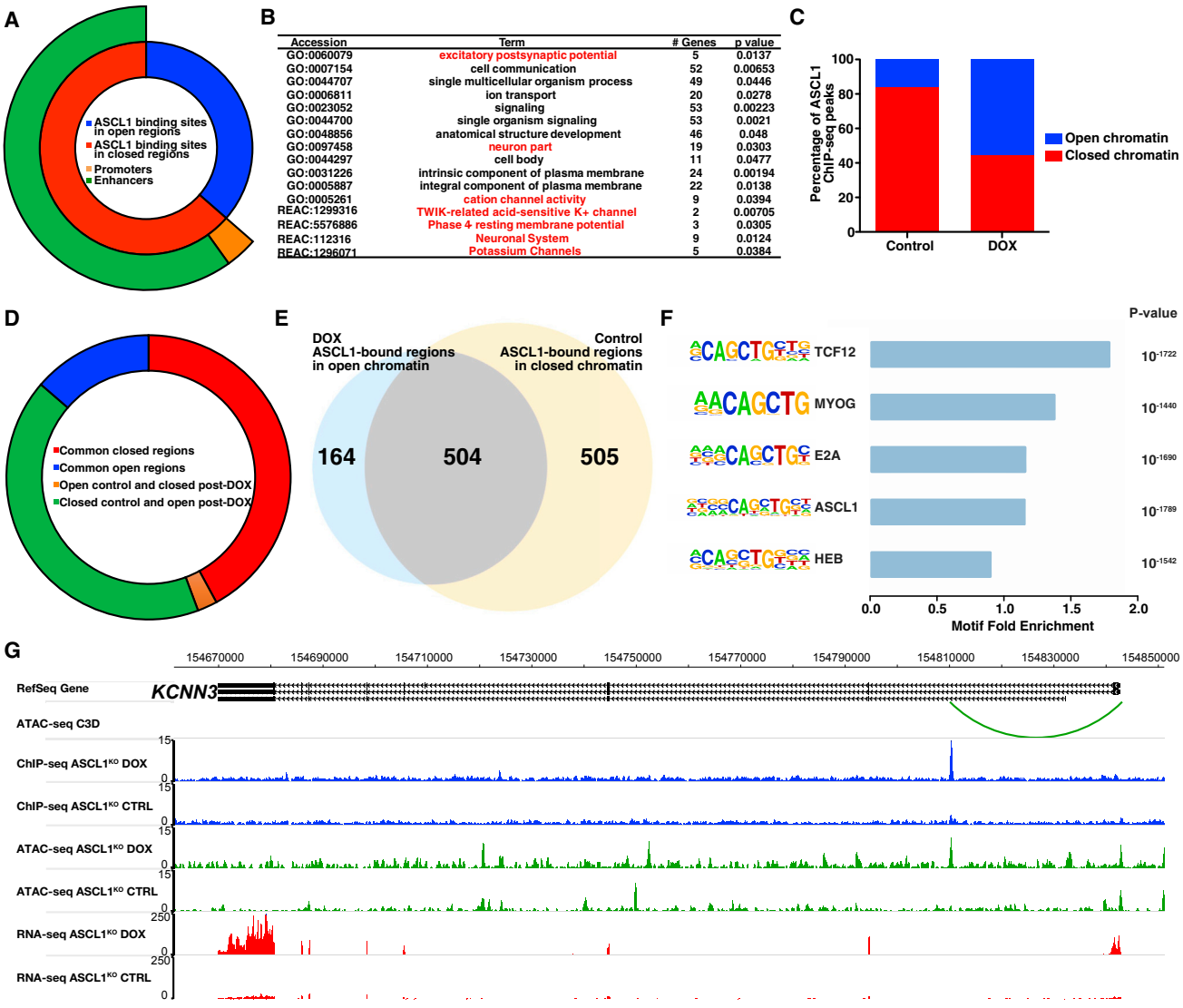

Figure 7. ASCL1 Binds to Closed Enhancer Regions of Neuronal Target Genes

(A) Doughnut plots displaying the proportion of ASCL1 binding sites in open and closed regions in GBM (n = 11 tumors).

(B) gProfiler analysis reveal ASCL1 binds to enhancers of genes involved in neuronal function (red).

(C) Distribution of ASCL1-bound regions in open and closed regions of ASCL1^{KO} GSCs treated with DOX compared to control.

(D) Doughnut plots displaying the proportion of open and closed regions that are bound by ASCL1 in ASCL1^{KO} GSCs in DOX versus control conditions.

(E) Venn diagram displaying unique and shared regions of open chromatin bound by ASCL1 in DOX conditions (blue) compared to ASCL1 binding sites mapped to closed regions in the control setting (yellow).

(E) Motif enrichment analysis of open regions in ASCL1^{KO} GSCs treated with DOX.

(F) Alignment data displaying ASCL1 binding (blue) within a newly opened region (green) predicted to interact (green arc) with the promoter region of *KCNN3* (black) and upregulate expression (red) under DOX conditions.

See also Figure S6 and Table S6.

genes, including inwardly rectifying potassium channels that were part of the upregulated gene set from RNA-seq analysis of *ASCL1* overexpression (Figure S6E). Together, these analyses confirm the critical role of ASCL1 in mediating pan-neuronal differentiation of ASCL1^{hi} GSCs.

As we found that most ASCL1 binding sites occur mostly in intergenic regions, consistent with previous reports of ASCL1 binding enhancer regions (Raposo et al., 2015; Webb et al., 2013) and emerging studies suggesting that ASCL1 functions as a pioneer factor (Raposo et al., 2015; Treutlein et al., 2016), we sought to determine whether ASCL1 binding sites occurred in regions of accessible or closed chromatin in GSCs. To do so, we performed assay for transposase-accessible chromatin sequencing (ATAC-seq) of 11 GSC cultures (five ASCL1^{hi} and six ASCL1^{lo}) identifying 141,231 regions accessible in at least one GSC culture. Of those, a total of 1,217 overlap ASCL1 binding sites (Figure 7A). The remaining 2,124 ASCL1 binding sites were associated with closed chromatin in GSCs (Figure 7A). To

test whether these ASCL1 sites in closed regions of chromatin could regulate genes required for neuronal differentiation, we identified their putative targets. A total of 549 promoters were associated with ASCL1 binding in closed chromatin. This corresponded to 123 directly bound promoters and 426 predicted to physically interact with distal ASCL1 bound sites based on the C3D analysis ($R > 0.5$) (Bailey et al., 2015). This corresponds to a total set of 509 genes (Table S6). Gene ontology analysis of these putative ASCL1 target genes revealed terms relating to neuronal function (Figure 7B) and included genes involved in excitatory postsynaptic potential, neuronal cell components, cation channel activity, and resting membrane potential.

The fact that ASCL1 binding following its overexpression occurred in regions of closed chromatin argues for a role of ASCL1 as a pioneer factor (Zaret and Carroll, 2011). This was assessed by performing ATAC-seq of ASCL1^{KO} GSCs before and after induction of *ASCL1* expression. Comparing the ATAC-seq chromatin profiles with ASCL1 ChIP-seq data, we found that ASCL1 binding sites are associated with more regions of closed chromatin in the un-induced state compared to DOX (Figures 7C and 7D). Approximately 85% of closed regions in the control setting co-occur with ASCL1 binding sites. This proportion is reduced by half under DOX conditions (Figures 7C and 7D). Interestingly, upon *ASCL1* induction, we found that 75.4% of regions of accessible chromatin bound by ASCL1 were derived from regions closed prior to *ASCL1* induction. Specifically, out of a total of 668 ASCL1-bound regions mapping to accessible chromatin after DOX induction, 504 regions are closed in the control setting (Figure 7E). In support of a direct DNA binding for ASCL1 to these regions, DNA recognition motif enrichment analysis in the accessible chromatin specific to the DOX-treatment condition revealed the presence of the ASCL1 motif, a finding that was not observed in the control setting (Figures 7F and S6F). A case example is the frequently closed region in GBM, which includes the genomic locus of a potassium channel gene, *KCNN3* (Figure 7G). C3D analysis of our ChIP-seq data revealed that ASCL1 binds in a region predicted to interact with the promoter region of *KCNN3*. ATAC-seq data confirmed this region is accessible and overlaps with ASCL1-binding in DOX-treated ASCL1^{KO} cells. RNA-seq analysis revealed *ASCL1* overexpression results in increased expression of *KCNN3*.

Overall, we demonstrate that ASCL1 binds to both promoter regions as well as enhancer regions of neuronal target genes. The majority of regions bound by ASCL1 were associated with closed chromatin in primary GSC cultures, prior to *ASCL1* overexpression, and acquired accessibility upon *ASCL1* overexpression, supporting its role as a pioneering factor. Combined with our previous functional data, ASCL1 reorganization of chromatin and activation of downstream target genes directly converts the cell state of GSCs to a more differentiated state, with strong emphasis on neuronal fate.

DISCUSSION

Loss of proliferation control and unregulated self-renewal have been the focus for anti-GBM therapies, but the recognition that these tumors are driven by subpopulations of cells with stem cell properties suggests that differentiation failure may be an additional and necessary hallmark of this highly malignant disease. Interestingly, our group has observed that the proliferation properties of normal NSCs and GSCs seem surprisingly similar in vitro, and their phenotypic differences are more strikingly revealed when tested for differentiation and tumorigenic potential. Restoration of differentiation control is predicted to restrict clonal expansion of tumor stem cell populations by enforcing their conversion into cells that acquire more mature states and that lose proliferative capacity. In medulloblastoma, differentiated tumor cells are short-lived and do not contribute to tumor growth, also suggesting differentiation in a neoplastic context may help to eliminate stem cell progeny (Vanner et al., 2014). In this study, we demonstrate that a subset of GBM cells from patient samples can be coaxed to produce neurons in response to small molecules that target Notch signaling, raising the possibility for directed differentiation therapy for patients with ASCL1^{hi} GSCs.

GBM cells derived from primary tumors have been known to display variable response to differentiation cues, but reasons for responsiveness and mechanisms governing differentiated cell fate competency remain unclear. Targeting the Notch pathway in GBM reduces cell proliferation and tumor-initiating properties (Chu et al., 2013; Fan et al., 2010). However, reports of poor responses to Notch inhibition in vitro (Saito et al., 2014) and in vivo (Giachino et al., 2015) in some samples likely explain differential patient responses in clinical trials (Krop et al., 2012; Yahyanejad et al., 2016). Thus, stratification of patients into subgroups that predict treatment response could be a breakthrough for patients. We found that patients that respond to Notch inhibition can be stratified by determining *ASCL1* expression levels. This group retains neurogenic capacity and responsiveness to therapy that enhances ASCL1-mediated neuronal differentiation. Other agents, such as glutamate receptor agonists (Andersen et al., 2014) have been shown to increase *ASCL1* expression in normal NSCs suggesting additional pathways that modify *ASCL1* expression may have clinical opportunity in this GBM patient subset.

Astrocytes are capable of re-entering the cell cycle in response to injury in the process of gliosis. Experimentally, following brain tissue wounding, astrocytes can be reprogrammed into cells that have neurogenic regenerative potential. For example, in ischemic stroke models, infarction triggers the appearance of up to ~70% Ascl1^{+} cells along the border of the lesion that sequentially generates Dcx^{+} neuroblasts and mature NeuN^{+} neurons, a regenerative process dependent on suppression of Notch signaling (Magnusson et al., 2014). In contrast, differentiated neurons of the brain do not turn over in brain homeostasis, do not demonstrate proliferative responses to injury, and are resistant to transformation experimentally (Alcantara Llaguno et al., 2009; Friedmann-Morvinski et al., 2012). The blocked differentiation phenotype has, in part, been shown to be due to deletion of genes that promote differentiation or also in loss of function of p53/Pten (Hu et al., 2013, 2016; Zheng et al., 2008). Restoration of expression of A2BP1 (Hu et al., 2013) or enforced expression of NGN2 (Su et al., 2014) reduced tumorigenic properties of GBM cells associated with cellular differentiation into neuronal fate. In GSCs treated with a short course of DOX to increase *ASCL1*, we show that these cells remained out of cycle despite being in pro-proliferative growth conditions, indicating that GSCs that acquire neuronal state are highly resistant to

re-entering the cell cycle. Enforced expression of *ASCL1* in vivo was able to direct ASCL1^{lo} GSCs into the neuronal lineage, indicating that these tumors could be made to be differentiation-competent resulting in improved survival. Collectively, these data suggest that steering differentiation of GSCs into mature neuronal cell types may result in a more stable state that resists proliferation and suppresses the neoplastic phenotype.

In mouse NSCs, Ascl1 has been shown to promote proliferation of quiescent cells, but thereafter, Ascl1 drives differentiation of progenitors. Loss of *Ascl1* expression in mice causes severe decreases in numbers of differentiated neurons. These apparently contradictory roles for Ascl1 function depend on the context of expression in the normal NSC hierarchy, first, promotion of proliferation of stem cells leads to adequate numbers of proliferating progenitor progeny, which then use Ascl1 to drive differentiation into neurons (Castro et al., 2011; Imayoshi et al., 2013). Based on our loss-of-function experiments, ASCL1 does not seem to maintain GSC proliferation and self-renewal that suggests different cellular contexts may dictate ASCL1 function (Rheinbay et al., 2013). Indeed, context-dependent roles in different primary GSC culture systems, threshold levels of ASCL1, and/or post-translational regulation may represent important rheostat controls that dictate ASCL1's role in promoting proliferation or differentiation (Castro et al., 2011; Imayoshi et al., 2013; Li et al., 2014). In human GBM, cells that have higher steady-state *ASCL1* levels can increase *ASCL1* expression and direct neuronal differentiation, but knock out of ASCL1 had no effect on proliferation or tumorigenicity. Therefore, ASCL1^{hi} GSCs may reflect tumor cells that are entrapped in a progenitor state, which then demonstrate an appropriate context to guide neuronal differentiation when *ASCL1* levels are further increased. In the context of inhibition of Notch signaling or overexpression, ASCL1 plays a dominant role in promoting neuronal differentiation in GBM. Supporting a role of ASCL1 to drive differentiation, ChIP-seq for ASCL1 demonstrated preferential binding target genes involved neuronal differentiation over cell-cycle targets. In GSCs, enforced *ASCL1*, like direct neuronal reprogramming of somatic cells, promotes neuronal differentiation in the absence of cell proliferation (Chanda et al., 2014; Pang et al., 2011; Wapinski et al., 2013).

ASCL1 binds to chromatin to activate gene expression. In particular, ASCL1 is capable of functioning as a pioneer factor, binding then opening regions of closed chromatin, leading to the orchestration of expression of neuronal fate genes that promote differentiation. These data are consistent with previous reports of mouse Ascl1 capable of binding to regions depleted of nucleosome-free DNA as determined by formaldehyde-assisted isolation of regulatory elements sequencing (FAIRE-seq) analysis (Raposo et al., 2015; Wapinski et al., 2013). In the context of human GBM, we determined that two-thirds of all ASCL1 binding sites are contained within closed regions, and ASCL1 functions to promote chromatin accessibility at enhancer regions to transcriptionally activate neuronal target genes. These data demonstrate a potent action of this transcription factor to reverse failed differentiation in GBM, shifting chromatin from unfavorable states of differentiation to active states. ChIP-seq also showed that ASCL1 suppressed glial and neural precursor cell fate by increasing expression of genes such as *NKX6-2*, *HMGA2*, *GPR37L1*, and *MYT1*. Interestingly, MyT1 has been shown to directly repress Notch signaling component genes (i.e., *Notch1*, *Hes1*, *Sox2*, *Id3*, and *Olig1*) during mouse neurogenesis (Vasconcelos et al., 2016). Therefore, ASCL1 initiates a coordinated fate determination program, simultaneously suppressing precursor and glial fate in favor of neuronal fate.

The neoplastic environment is not necessarily hostile to directed fate specification consistent with the neurogenic effects of expression of *ASCL1* in unexpected cell types such as hepatocytes (Marro et al., 2011). ASCL1^{hi} GSCs retain a developmental neurogenic capacity, their differentiation potential can be unmasked by several strategies and suggests further emphasis should be made in identifying other agents or pathways that promote neuronal lineage differentiation. Moreover, enforced expression of *ASCL1* can restore differentiation capacity of ASCL1^{lo} GSCs, suggesting that blocks to differentiation can be overcome in these GSCs. We are hopeful that this work brings renewed attention to the potential of differentiation therapy in a subgroup of GBM patients and leads to further work exploring neurogenesis in the GBM context for therapeutic application.

STAR★METHODS

Detailed methods are provided in the online version of this paper and include the following:

- KEY RESOURCES TABLE
- CONTACT FOR REAGENT AND RESOURCE SHARING
- EXPERIMENTAL MODEL AND SUBJECT DETAILS
  - Patient Samples and Primary Cell Cultures
  - Sample Nomenclature
  - Animals
  - Flies
- METHOD DETAILS
  - Transfections
  - Tissue and Cell Staining and Microscopy
  - In Vitro Differentiation Assay
  - In Vitro Cell Proliferation Assay
  - In Vitro Limiting Dilution Assay
  - In Vitro Live-Cell Imaging
  - In Vivo Transplantation Assay and Treatment
  - In Vivo Secondary Transplantation Assay
  - Experimental Design
  - RNA Sequencing Analysis
  - ChIP Sequencing Analysis
  - ATAC Sequencing Analysis
  - Motif Enrichment Analysis
- QUANTIFICATION AND STATISTICAL ANALYSIS
  - Details and Number of Samples Analyzed
- DATA AND SOFTWARE AVAILABILITY

SUPPLEMENTAL INFORMATION

Supplemental Information includes seven figures, seven tables, and one movie and can be found with this article online at http://dx.doi.org/10.1016/j.stem.2017.06.004.

AUTHOR CONTRIBUTIONS

Conceptualizations, N.I.P. and P.B.D.; Methodology, N.I.P. and P.B.D.; Formal Analysis, P.G. and K.D.; Investigation, N.I.P., R.F.M.A., E. Langille, M.O.C.,

X.L., F.J.C., R.J.V., E. Ling, H.W., G.A., P.P., L.L., and M.K.; Resources, L.L., I.D.C., M.D.C., M.B., S.D., C.H.A., V.V., and G.B.; Writing – Original Draft, N.I.P. and P.B.D.; Writing – Review & Editing, N.I.P., P.B.D., P.G., H.S., X.L., K.D., M.L., S.A., and X.H.; Supervision, P.B.D., M.L., S.A., and X.H.; Funding Acquisition, N.I.P. and P.B.D.

ACKNOWLEDGMENTS

We would like to thank the SickKids-UHN Flow Cytometry Facility, The Centre for Applied Genomics (TCAG), the Princess Margaret Genomics Centre (https://www.pmgenomics.ca), and the Princess Margaret Bioinformatics group for contributions to this work. We thank Francois Guillemot for the DN-ASCL1 and ASCL1 reporter constructs, Jon Aster for the DN-MAML construct, and Michael McGrew for the Piggybac transposon inducible expression system. Research was supported by SU2C Canada Cancer Stem Cell Dream Team Research Funding (SU2C-AACR-DT-19-15) provided by the Government of Canada through Genome Canada and the Canadian Institute of Health Research (142434), with supplemental support from the Ontario Institute for Cancer Research through funding provided by the Government of Ontario. Stand Up To Cancer Canada is a program of the Entertainment Industry Foundation Canada. Research funding is administered by the American Association for Cancer Research International-Canada, the scientific partner of SU2C Canada. We thank the Hospital for Sick Children Foundation, Jessica's Footprint, Hopeful Minds Foundation, and B.R.A.I.N. Child. P.B.D. holds a Garron Family Chair in Childhood Cancer Research at The Hospital for Sick Children, and M.L. holds a Young Investigator Award from the Ontario Institute for Cancer Research, a new investigator salary award from the Canadian Institute of Health Research (CIHR), and a Movember Rising Star award from Prostate Cancer Canada (PCC) (RS2014-04). N.I.P. is supported by The Ontario Graduate Scholarship, The Hospital for Sick Children, and The Garron Family Cancer Centre. P.G. is supported by a CIHR Fellowship (MFE 338954). The Structural Genomics Consortium is funded by AbbVie, Bayer, Boehringer Ingelheim, GSK, Genome Canada, Ontario Genomics Institute, Janssen, Lilly, Merck, Novartis, the Government of Ontario, Pfizer, Takeda, and the Wellcome Trust.

Received: January 5, 2017
Revised: May 10, 2017
Accepted: June 15, 2017
Published: July 13, 2017

REFERENCES

Alcantara Llaguno, S., Chen, J., Kwon, C.H., Jackson, E.L., Li, Y., Burns, D.K., Alvarez-Buylla, A., and Parada, L.F. (2009). Malignant astrocytomas originate from neural stem/progenitor cells in a somatic tumor suppressor mouse model. Cancer Cell *15*, 45–56.

Alcantara Llaguno, S.R., Wang, Z., Sun, D., Chen, J., Xu, J., Kim, E., Hatanpaa, K.J., Raisanen, J.M., Burns, D.K., Johnson, J.E., and Parada, L.F. (2015). Adult lineage-restricted CNS progenitors specify distinct glioblastoma subtypes. Cancer Cell *28*, 429–440.

Andersen, J., Urbán, N., Achimastou, A., Ito, A., Simic, M., Ullom, K., Martynoga, B., Lebel, M., Göritz, C., Frisén, J., et al. (2014). A transcriptional mechanism integrating inputs from extracellular signals to activate hippocampal stem cells. Neuron *83*, 1085–1097.

Bailey, S.D., Zhang, X., Desai, K., Aid, M., Corradin, O., Cowper-Sal Lari, R., Akhtar-Zaidi, B., Scacheri, P.C., Haibe-Kains, B., and Lupien, M. (2015). ZNF143 provides sequence specificity to secure chromatin interactions at gene promoters. Nat. Commun. *2*, 6186.

Bardehle, S., Krüger, M., Buggenthin, F., Schwausch, J., Ninkovic, J., Clevers, H., Snippert, H.J., Theis, F.J., Meyer-Luehmann, M., Bechmann, I., et al. (2013). Live imaging of astrocyte responses to acute injury reveals selective juxtavascular proliferation. Nat. Neurosci. *16*, 580–586.

Berninger, B., Guillemot, F., and Götz, M. (2007). Directing neurotransmitter identity of neurones derived from expanded adult neural stem cells. Eur. J. Neurosci. *25*, 2581–2590.

Bertrand, N., Castro, D.S., and Guillemot, F. (2002). Proneural genes and the specification of neural cell types. Nat. Rev. Neurosci. *3*, 517–530.

Brennan, C.W., Verhaak, R.G., McKenna, A., Campos, B., Noushmehr, H., Salama, S.R., Zheng, S., Chakravarty, D., Sanborn, J.Z., Berman, S.H., et al.; TCGA Research Network (2013). The somatic genomic landscape of glioblastoma. Cell *155*, 462–477.

Buenrostro, J.D., Giresi, P.G., Zaba, L.C., Chang, H.Y., and Greenleaf, W.J. (2013). Transposition of native chromatin for fast and sensitive epigenomic profiling of open chromatin, DNA-binding proteins and nucleosome position. Nat Methods *10*, 1213–1218.

Carén, H., Stricker, S.H., Bulstrode, H., Gagrica, S., Johnstone, E., Bartlett, T.E., Feber, A., Wilson, G., Teschendorff, A.E., Bertone, P., et al. (2015). Glioblastoma stem cells respond to differentiation cues but fail to undergo commitment and terminal cell-cycle arrest. Stem Cell Reports *5*, 829–842.

Carlsson, S.K., Brothers, S.P., and Wahlestedt, C. (2014). Emerging treatment strategies for glioblastoma multiforme. EMBO Mol. Med. *6*, 1359–1370.

Castella, P., Wagner, J.A., and Caudy, M. (1999). Regulation of hippocampal neuronal differentiation by the basic helix-loop-helix transcription factors HES-1 and MASH-1. J. Neurosci. Res. *56*, 229–240.

Castro, D.S., Skowronska-Krawczyk, D., Armant, O., Donaldson, I.J., Parras, C., Hunt, C., Critchley, J.A., Nguyen, L., Gossler, A., Göttgens, B., et al. (2006). Proneural bHLH and Brn proteins coregulate a neurogenic program through cooperative binding to a conserved DNA motif. Dev. Cell *11*, 831–844.

Castro, D.S., Martynoga, B., Parras, C., Ramesh, V., Pacary, E., Johnston, C., Drechsel, D., Lebel-Potter, M., Garcia, L.G., Hunt, C., et al. (2011). A novel function of the proneural factor Ascl1 in progenitor proliferation identified by genome-wide characterization of its targets. Genes Dev. *25*, 930–945.

Chanda, S., Ang, C.E., Davila, J., Pak, C., Mall, M., Lee, Q.Y., Ahlenius, H., Jung, S.W., Südhof, T.C., and Wernig, M. (2014). Generation of induced neuronal cells by the single reprogramming factor ASCL1. Stem Cell Reports *3*, 282–296.

Chen, J., Li, Y., Yu, T.S., McKay, R.M., Burns, D.K., Kernie, S.G., and Parada, L.F. (2012). A restricted cell population propagates glioblastoma growth after chemotherapy. Nature *488*, 522–526.

Chu, Q., Orr, B.A., Semenkow, S., Bar, E.E., and Eberhart, C.G. (2013). Prolonged inhibition of glioblastoma xenograft initiation and clonogenic growth following in vivo Notch blockade. Clin. Cancer Res. *19*, 3224–3233.

Cline, M.S., Smoot, M., Cerami, E., Kuchinsky, A., Landys, N., Workman, C., Christmas, R., Avila-Campilo, I., Creech, M., Gross, B., et al. (2007). Integration of biological networks and gene expression data using Cytoscape. Nat. Protoc. *2*, 2366–2382.

Fan, X., Khaki, L., Zhu, T.S., Soules, M.E., Talsma, C.E., Gul, N., Koh, C., Zhang, J., Li, Y.M., Maciaczyk, J., et al. (2010). NOTCH pathway blockade depletes CD133-positive glioblastoma cells and inhibits growth of tumor neurospheres and xenografts. Stem Cells *28*, 5–16.

Friedmann-Morvinski, D., Bushong, E.A., Ke, E., Soda, Y., Marumoto, T., Singer, O., Ellisman, M.H., and Verma, I.M. (2012). Dedifferentiation of neurons and astrocytes by oncogenes can induce gliomas in mice. Science *338*, 1080–1084.

Gallo, M., Coutinho, F.J., Vanner, R.J., Gayden, T., Mack, S.C., Murison, A., Remke, M., Li, R., Takayama, N., Desai, K., et al. (2015). MLL5 orchestrates a cancer self-renewal state by repressing the histone variant H3.3 and globally reorganizing chromatin. Cancer Cell *28*, 715–729.

Giachino, C., Boulay, J.L., Ivanek, R., Alvarado, A., Tostado, C., Lugert, S., Tchorz, J., Coban, M., Mariani, L., Bettler, B., et al. (2015). A tumor suppressor function for Notch signaling in forebrain tumor subtypes. Cancer Cell *28*, 730–742.

Glover, J.D., Taylor, L., Sherman, A., Zeiger-Poli, C., Sang, H.M., and McGrew, M.J. (2013). A novel piggyback transposon inducible expression system identifies a role for AKT signalling in primordial germ cell migration. PLoS One *8*, e77222.

Gravendeel, L.A., Kouwenhoven, M.C., Gevaert, O., de Rooi, J.J., Stubbs, A.P., Duijm, J.E., Daemen, A., Bleeker, F.E., Bralten, L.B., Kloosterhof, N.K.,

et al. (2009). Intrinsic gene expression profiles of gliomas are a better predictor of survival than histology. Cancer Res. *69*, 9065–9072.

Heinz, S., Benner, C., Spann, N., Bertolino, E., Lin, Y.C., Laslo, P., Cheng, J.X., Murre, C., Singh, H., and Glass, C.K. (2010). Simple combinations of lineage-determining transcription factors prime cis-regulatory elements required for macrophage and B cell identities. Mol. Cell. *38*, 576–589.

Hu, Y., and Smyth, G.K. (2009). ELDA: extreme limiting dilution analysis for comparing depleted and enriched populations in stem cell and other assays. J. Immunol. Methods *347*, 70–78.

Hu, J., Ho, A.L., Yuan, L., Hu, B., Hua, S., Hwang, S.S., Zhang, J., Hu, T., Zheng, H., Gan, B., et al. (2013). From the Cover: Neutralization of terminal differentiation in gliomagenesis. Proc. Natl. Acad. Sci. USA *110*, 14520–14527.

Hu, B., Wang, Q., Wang, Y.A., Hua, S., Sauve, C.G., Ong, D., Lan, Z.D., Chang, Q., Ho, Y.W., Monasterio, M.M., et al. (2016). Epigenetic activation of WNT5A drives glioblastoma stem cell differentiation and invasive growth. Cell *167*, 1281–1295.

Imayoshi, I., Isomura, A., Harima, Y., Kawaguchi, K., Kori, H., Miyachi, H., Fujiwara, T., Ishidate, F., and Kageyama, R. (2013). Oscillatory control of factors determining multipotency and fate in mouse neural progenitors. Science *342*, 1203–1208.

Kageyama, R., Ohtsuka, T., Hatakeyama, J., and Ohsawa, R. (2005). Roles of bHLH genes in neural stem cell differentiation. Exp. Cell Res. *306*, 343–348.

Kim, E.J., Ables, J.L., Dickel, L.K., Eisch, A.J., and Johnson, J.E. (2011). Ascl1 (Mash1) defines cells with long-term neurogenic potential in subgranular and subventricular zones in adult mouse brain. PLoS ONE *6*, e18472.

Krop, I., Demuth, T., Guthrie, T., Wen, P.Y., Mason, W.P., Chinnaiyan, P., Butowski, N., Groves, M.D., Kesari, S., Freedman, S.J., et al. (2012). Phase I pharmacologic and pharmacodynamic study of the gamma secretase (Notch) inhibitor MK-0752 in adult patients with advanced solid tumors. J. Clin. Oncol. *30*, 2307–2313.

Langmead, B., and Salzberg, S.L. (2012). Fast gapped-read alignment with Bowtie 2. Nat. Methods *9*, 357–359.

Lee, J., Son, M.J., Woolard, K., Donin, N.M., Li, A., Cheng, C.H., Kotliarova, S., Kotliarov, Y., Walling, J., Ahn, S., et al. (2008). Epigenetic-mediated dysfunction of the bone morphogenetic protein pathway inhibits differentiation of glioblastoma-initiating cells. Cancer Cell *13*, 69–80.

Li, H., Handsaker, B., Wysoker, A., Fennell, T., Ruan, J., Homer, N., Marth, G., Abecasis, G., and Durbin, R.; 1000 Genome Project Data Processing Subgroup (2009). The Sequence Alignment/Map format and SAMtools. Bioinformatics *25*, 2078–2079.

Li, S., Mattar, P., Dixit, R., Lawn, S.O., Wilkinson, G., Kinch, C., Eisenstat, D., Kurrasch, D.M., Chan, J.A., and Schuurmans, C. (2014). RAS/ERK signaling controls proneural genetic programs in cortical development and gliomagenesis. J. Neurosci. *34*, 2169–2190.

Magnusson, J.P., Göritz, C., Tatarishvili, J., Dias, D.O., Smith, E.M., Lindvall, O., Kokaia, Z., and Frisén, J. (2014). A latent neurogenic program in astrocytes regulated by Notch signaling in the mouse. Science *346*, 237–241.

Marro, S., Pang, Z.P., Yang, N., Tsai, M.C., Qu, K., Chang, H.Y., Südhof, T.C., and Wernig, M. (2011). Direct lineage conversion of terminally differentiated hepatocytes to functional neurons. Cell Stem Cell *9*, 374–382.

McCarthy, D.J., Chen, Y., and Smyth, G.K. (2012). Differential expression analysis of multifactor RNA-seq experiments with respect to biological variation. Nucleic Acids Res. *40*, 4288–4297.

Merico, D., Isserlin, R., Stueker, O., Emili, A., and Bader, G.D. (2010). Enrichment map: a network-based method for gene-set enrichment visualization and interpretation. PLoS One *5*, e13984.

Meyer, M., Reimand, J., Lan, X., Head, R., Zhu, X., Kushida, M., Bayani, J., Pressey, J.C., Lionel, A.C., Clarke, I.D., et al. (2015). Single cell-derived clonal analysis of human glioblastoma links functional and genomic heterogeneity. Proc. Natl. Acad. Sci. USA *112*, 851–856.

Montague, T.G., Cruz, J.M., Gagnon, J.A., Church, G.M., and Valen, E. (2014). CHOPCHOP: a CRISPR/Cas9 and TALEN web tool for genome editing. Nucleic Acids Res. *42*, W401–W407.

Mootha, V.K., Bunkenborg, J., Olsen, J.V., Hjerrild, M., Wisniewski, J.R., Stahl, E., Bolouri, M.S., Ray, H.N., Sihag, S., Kamal, M., et al. (2003). Integrated analysis of protein composition, tissue diversity, and gene regulation in mouse mitochondria. Cell *115*, 629–640.

Pang, Z.P., Yang, N., Vierbuchen, T., Ostermeier, A., Fuentes, D.R., Yang, T.Q., Citri, A., Sebastiano, V., Marro, S., Südhof, T.C., and Wernig, M. (2011). Induction of human neuronal cells by defined transcription factors. Nature *476*, 220–223.

Patel, A.P., Tirosh, I., Trombetta, J.J., Shalek, A.K., Gillespie, S.M., Wakimoto, H., Cahill, D.P., Nahed, B.V., Curry, W.T., Martuza, R.L., et al. (2014). Single-cell RNA-seq highlights intratumoral heterogeneity in primary glioblastoma. Science *344*, 1396–1401.

Piccirillo, S.G., Reynolds, B.A., Zanetti, N., Lamorte, G., Binda, E., Broggi, G., Brem, H., Olivi, A., Dimeco, F., and Vescovi, A.L. (2006). Bone morphogenetic proteins inhibit the tumorigenic potential of human brain tumour-initiating cells. Nature *444*, 761–765.

Pollard, S.M., Yoshikawa, K., Clarke, I.D., Danovi, D., Stricker, S., Russell, R., Bayani, J., Head, R., Lee, M., Bernstein, M., et al. (2009). Glioma stem cell lines expanded in adherent culture have tumor-specific phenotypes and are suitable for chemical and genetic screens. Cell Stem Cell *4*, 568–580.

Quinlan, A.R., and Hall, I.M. (2010). BEDTools: a flexible suite of utilities for comparing genomic features. Bioinformatics *26*, 841–842.

Raposo, A.A., Vasconcelos, F.F., Drechsel, D., Marie, C., Johnston, C., Dolle, D., Bithell, A., Gillotin, S., van den Berg, D.L., Ettwiller, L., et al. (2015). Ascl1 coordinately regulates gene expression and the chromatin landscape during neurogenesis. Cell Rep. http://dx.doi.org/10.1016/j.celrep.2015.02.025.

Read, R.D., Cavenee, W.K., Furnari, F.B., and Thomas, J.B. (2009). A Drosophila model for EGFR-Ras and PI3K-dependent human glioma. PLoS Genet. *5*, e1000374.

Rheinbay, E., Suvà, M.L., Gillespie, S.M., Wakimoto, H., Patel, A.P., Shahid, M., Oksuz, O., Rabkin, S.D., Martuza, R.L., Rivera, M.N., et al. (2013). An aberrant transcription factor network essential for Wnt signaling and stem cell maintenance in glioblastoma. Cell Rep. *3*, 1567–1579.

Robinson, M.D., McCarthy, D.J., and Smyth, G.K. (2010). edgeR: a bioconductor package for differential expression analysis of digital gene expression data. Bioinformatics *26*, 139–140.

Saito, N., Fu, J., Zheng, S., Yao, J., Wang, S., Liu, D.D., Yuan, Y., Sulman, E.P., Lang, F.F., Colman, H., et al. (2014). A high Notch pathway activation predicts response to γ secretase inhibitors in proneural subtype of glioma tumor-initiating cells. Stem Cells *32*, 301–312.

Shin, H., Liu, T., Manrai, A.K., and Liu, X.S. (2009). CEAS: cis-regulatory element annotation system. Bioinformatics *25*, 2605–2606.

Singh, S.K., Hawkins, C., Clarke, I.D., Squire, J.A., Bayani, J., Hide, T., Henkelman, R.M., Cusimano, M.D., and Dirks, P.B. (2004). Identification of human brain tumour initiating cells. Nature *432*, 396–401.

Su, Z., Zang, T., Liu, M.L., Wang, L.L., Niu, W., and Zhang, C.L. (2014). Reprogramming the fate of human glioma cells to impede brain tumor development. Cell Death Dis. *5*, e1463.

Subramanian, A., Tamayo, P., Mootha, V.K., Mukherjee, S., Ebert, B.L., Gillette, M.A., Paulovich, A., Pomeroy, S.L., Golub, T.R., Lander, E.S., and Mesirov, J.P. (2005). Gene set enrichment analysis: a knowledge-based approach for interpreting genome-wide expression profiles. Proc Natl Acad Sci USA *102*, 15545–15550.

Tirosh, I., Venteicher, A.S., Hebert, C., Escalante, L.E., Patel, A.P., Yizhak, K., Fisher, J.M., Rodman, C., Mount, C., Filbin, M.G., et al. (2016). Single-cell RNA-seq supports a developmental hierarchy in human oligodendroglioma. Nature *539*, 309–313.

Treutlein, B., Lee, Q.Y., Camp, J.G., Mall, M., Koh, W., Shariati, S.A., Sim, S., Neff, N.F., Skotheim, J.M., Wernig, M., and Quake, S.R. (2016). Dissecting

direct reprogramming from fibroblast to neuron using single-cell RNA-seq. Nature *534*, 391–395.

Vanner, R.J., Remke, M., Gallo, M., Selvadurai, H.J., Coutinho, F., Lee, L., Kushida, M., Head, R., Morrissy, S., Zhu, X., et al. (2014). Quiescent sox2(+) cells drive hierarchical growth and relapse in sonic hedgehog subgroup medulloblastoma. Cancer Cell *26*, 33–47.

Vasconcelos, F.F., Sessa, A., Laranjeira, C., Raposo, A.A., Teixeira, V., Hagey, D.W., Tomaz, D.M., Muhr, J., Broccoli, V., and Castro, D.S. (2016). MyT1 counteracts the neural progenitor program to promote vertebrate neurogenesis. Cell Rep. *17*, 469–483.

Vierbuchen, T., Ostermeier, A., Pang, Z.P., Kokubu, Y., Südhof, T.C., and Wernig, M. (2010). Direct conversion of fibroblasts to functional neurons by defined factors. Nature *463*, 1035–1041.

von Neubeck, C., Seidlitz, A., Kitzler, H.H., Beuthien-Baumann, B., and Krause, M. (2015). Glioblastoma multiforme: emerging treatments and stratification markers beyond new drugs. Br. J. Radiol. *88*, 20150354.

Wapinski, O.L., Vierbuchen, T., Qu, K., Lee, Q.Y., Chanda, S., Fuentes, D.R., Giresi, P.G., Ng, Y.H., Marro, S., Neff, N.F., et al. (2013). Hierarchical mechanisms for direct reprogramming of fibroblasts to neurons. Cell *155*, 621–635.

Webb, A.E., Pollina, E.A., Vierbuchen, T., Urbán, N., Ucar, D., Leeman, D.S., Martynoga, B., Sewak, M., Rando, T.A., Guillemot, F., et al. (2013). FOXO3 shares common targets with ASCL1 genome-wide and inhibits ASCL1-dependent neurogenesis. Cell Rep. *4*, 477–491.

Weng, A.P., Nam, Y., Wolfe, M.S., Pear, W.S., Griffin, J.D., Blacklow, S.C., and Aster, J.C. (2003). Growth suppression of pre-T acute lymphoblastic leukemia cells by inhibition of notch signaling. Mol. Cell. Biol. *23*, 655–664.

Wilkinson, G., Dennis, D., and Schuurmans, C. (2013). Proneural genes in neocortical development. Neuroscience *253*, 256–273.

Yahyanejad, S., King, H., Iglesias, V.S., Granton, P.V., Barbeau, L.M., van Hoof, S.J., Groot, A.J., Habets, R., Prickaerts, J., Chalmers, A.J., et al. (2016). NOTCH blockade combined with radiation therapy and temozolomide prolongs survival of orthotopic glioblastoma. Oncotarget *7*, 41251–41264.

Yoo, A.S., Sun, A.X., Li, L., Shcheglovitov, A., Portmann, T., Li, Y., Lee-Messer, C., Dolmetsch, R.E., Tsien, R.W., and Crabtree, G.R. (2011). MicroRNA-mediated conversion of human fibroblasts to neurons. Nature *476*, 228–231.

Zaret, K.S., and Carroll, J.S. (2011). Pioneer transcription factors: establishing competence for gene expression. Genes Dev. *25*, 2227–2241.

Zhang, Y., Liu, T., Meyer, C.A., Eeckhoute, J., Johnson, D.S., Bernstein, B.E., Nusbaum, C., Myers, R.M., Brown, M., Li, W., and Liu, X.S. (2008). Model-based analysis of ChIP-Seq (MACS). Genome Biol. *9*, R137.

Zheng, H., Ying, H., Yan, H., Kimmelman, A.C., Hiller, D.J., Chen, A.J., Perry, S.R., Tonon, G., Chu, G.C., Ding, Z., et al. (2008). Pten and p53 converge on c-Myc to control differentiation, self-renewal, and transformation of normal and neoplastic stem cells in glioblastoma. Cold Spring Harb. Symp. Quant. Biol. *73*, 427–437.

STAR★METHODS

KEY RESOURCES TABLE

REAGENT or RESOURCE	SOURCE	IDENTIFIER
Antibodies		
Anti-MASH1 antibody (clone 24B72D11.1)	BD Biosciences	Cat#556604; RRID: AB_396479
Anti-TUBB3 antibody (clone DM1A)	Sigma Aldrich	Cat#T9026; RRID: AB_477593
Anti-GFAP antibody (clone SMI21)	Covance Research Products	Cat#SMI-21R; RRID: AB_509978
Anti-NESTIN antibody	Millipore	Cat#AB5922; RRID: AB_11211011
Anti-SOX2 antibody (clone 245610)	R and D Systems	Cat#MAB2018; RRID: AB_358009
Anti-VGLUT1 antibody	Synaptic Systems	Cat#135 303C3; RRID: AB_887874
Anti-MAP-2 antibody (clone ap20)	Millipore	Cat#MAB3418; RRID: AB_94856
Anti-NEUN antibody (clone A60)	Millipore	Cat#MAB377; RRID: AB_2298772
Anti-S-100 beta chain antibody (clone sb6)	Santa Cruz Biotechnology	Cat#sc-58841; RRID: AB_632378
Anti-cleaved caspase-3 (Asp175) antibody	Cell Signaling Technology	Cat#9661; RRID: AB_2341188
Anti-GABA antibody	Sigma Aldrich	Cat#A2052; RRID: AB_477652
Anti-Ki67 antibody (clone MIB-1)	Agilent	Cat#M724029
Anti-Elav antibody	Developmental Studies Hybridoma Bank	Cat#78A10; RRID: SCR_013527
Anti-Repo antibody	Developmental Studies Hybridoma Bank	Cat#8D12; RRID: SCR_013527
Anti-cyclin B antibody	Developmental Studies Hybridoma Bank	Cat#F2F4-S; RRID: SCR_013527
Bacterial and Virus Strains		
Plasmid: Dominant negative ASCL1	Francois Guillemot; Castro et al., 2006	N/A
Plasmid: ASCL1 Luciferase Reporter	Francois Guillemot; Castro et al., 2006	N/A
Plasmid: pSpCas9(BB)-2A-GFP (PX458)	Addgene	Plasmid #48138
Plasmid: pSpCas9(BB)-2A-GFP (PX458) – ASCL1 gRNA #1	This paper	N/A
Plasmid: pSpCas9(BB)-2A-GFP (PX458) – ASCL1 gRNA #2	This paper	N/A
Plasmid: phASCL1-N106	Addgene	plasmid #31781
Plasmid: PB-Tet-ON	Michael McGrew; Glover et al., 2013	N/A
Plasmid: HyBase	Wellcome Trust Sanger Institute	Hinxton #515119
Plasmid: PB-Tet-ON-ASCL1	This paper	N/A
Biological Samples		
Primary GBM samples	University of Toronto Brain Tumor Bank; St. Michael's Hospital/Toronto Western Hospital	N/A
Primary HFNS samples	Research Centre for Women's and Infants' Health BioBank; Mount Sinai Hospital/UHN	N/A
Chemicals, Peptides, and Recombinant Proteins		
InSolution γ-Secretase Inhibitor X - Calbiochem	EMD Millipore	Cat#565771
γ-Secretase Inhibitor IX – CAS 208255-80-5 - Calbiochem	EMD Millipore	Cat#565770
NeuroCult NS-A Basal Medium (Human)	StemCell Technologies	Cat#05750
Recombinant human EGF	Sigma Aldrich	Cat#E9644
Basic FGF	StemCell Technologies	Cat#02634
Rodent Diet (2018, 625 Doxycycline)	Envigo	Cat#TD.01306
Puromycin dihydrochloride from *Streptomyces alboniger*	Sigma Aldrich	Cat#P8833
Doxycycline hyclate	Sigma Aldrich	Cat#D9891
Dimethyl sulfoxide	Sigma Aldrich	Cat#D2650

(*Continued on next page*)

Continued

REAGENT or RESOURCE	SOURCE	IDENTIFIER
Critical Commercial Assays		
Dual-Luciferase Reporter Assay System	Promega	Cat#E1910
ClickIT EdU Alexa Fluor 647 Imaging Kit	ThermoFisher Scientific	Cat#C10340
Trypan Blue Solution, 0.4%	ThermoFisher Scientific	Cat#15250061
Nucleofector Kits for Mouse Neural Stem Cells	Lonza	Cat#VVPG1004
ImmPress HRP Anti-Rabbit IgG (Peroxidase) Polymer Detection Kit, made in Horse	Vector Laboratories	Cat#MP-7401
Mouse Cell Depletion Kit	Miltenyi Biotec	Cat# 130-104-694
RNeasy Mini Kit	QIAGEN	Cat#74106
Nextera DNA Sample Preparation Kit	Illumina	FC-121-1030
Deposited Data		
Raw and analyzed exon microarray data	This paper	GEO: GSE87619
Raw and analyzed RNA-seq data	This paper	GEO: GSE87617; GSE87615
Raw and analyzed ChIP-seq data	This paper	GEO: GSE87618
Raw and analyzed ATAC-seq data	This paper	GEO: GSE90547; GSE96088
human reference genome NCBI build 37, GRCh37	Genome Reference Consortium	https://www.ncbi.nlm.nih.gov/projects/genome/assembly/grc/human/
Experimental Models: Organisms/Strains		
D. melanogaster: overexpression of ac: w*; P{UAS-ac}17/CyO	Bloomington Drosophila Stock Center	BDSC:26686; FlyBase: FBal0057942
D. melanogaster: overexpression of ASCL1: y1 w*; P{UAS-Hsap\ASCL1}3	Bloomington Drosophila Stock Center	BDSC:39711; FlyBase: FBti0147764
Mouse: NOD.Cg-Prkdc^{scid}Il2rg^{tm1Wjl}/SzJ (NSG)	The Jackson Laboratory	RRID:IMSR_JAX:005557
Oligonucleotides		
See Table S7 for oligonucleotide sequences.	N/A	N/A
Recombinant DNA		
Plasmid: Dominant negative ASCL1	Francois Guillemot; Castro et al., 2006	N/A
Plasmid: ASCL1 Luciferase Reporter	Francois Guillemot; Castro et al., 2006	N/A
Plasmid: pSpCas9(BB)-2A-GFP (PX458)	Addgene	Plasmid #48138
Plasmid: pLCKO	Addgene	Plasmid #73311
Plasmid: pSpCas9(BB)-2A-GFP (PX458) – ASCL1 gRNA #1	This paper	N/A
Plasmid: pSpCas9(BB)-2A-GFP (PX458) – ASCL1 gRNA #2	This paper	N/A
Plasmid: pLCKO-sgHES1	This paper	N/A
Plasmid: phASCL1-N106	Addgene	plasmid #31781
Plasmid: PB-Tet-ON	Michael McGrew; Glover et al., 2013	N/A
Plasmid: HyBase	Wellcome Trust Sanger Institute	Hinxton #515119
Plasmid: PB-Tet-ON-ASCL1	This paper	N/A
Software and Algorithms		
Analysis of TCGA dataset	R2: Genomics Analysis and Visualization Platform	http://r2.amc.nl
GSEA	(Mootha et al., 2003; Subramanian et al., 2005)	http://software.broadinstitute.org/gsea/index.jsp
Cytoscape	(Cline et al., 2007)	http://www.cytoscape.org
Enrichment Map	(Merico et al., 2010)	http://www.baderlab.org/Software/EnrichmentMap

(*Continued on next page*)

Continued

REAGENT or RESOURCE	SOURCE	IDENTIFIER
Tophat	N/A	https://ccb.jhu.edu/software/tophat/index.shtml
EdgeR	(McCarthy et al., 2012; Robinson et al., 2010)	http://bioconductor.org/packages/release/bioc/html/edgeR.html
Bowtie2	(Langmead and Salzberg, 2012)	http://bowtie-bio.sourceforge.net/bowtie2/index.shtml
Samtools	(Li et al., 2009)	http://samtools.sourceforge.net/
Bedtools	(Quinlan and Hall, 2010)	http://bedtools.readthedocs.io/en/latest/
MACS2	(Zhang et al., 2008)	https://github.com/taoliu/MACS/
CHOPCHOP	(Montague et al., 2014)	https://chopchop.rc.fas.harvard.edu/index.php
CRISPR Design	Zhang Lab, MIT 2015	http://crispr.mit.edu
Extreme Limiting Dilution Assay (ELDA)	(Hu and Smyth, 2009)	http://bioinf.wehi.edu.au/software/elda/
IncuCyte ZOOM NeuroTrack	Essen BioScience	N/A
GraphPad Prism 6	GraphPad Software, Inc.	N/A

CONTACT FOR REAGENT AND RESOURCE SHARING

Further information and requests for reagents may be directed to, and will be fulfilled by, the Lead Contact, Peter Dirks (peter.dirks@sickkids.ca).

EXPERIMENTAL MODEL AND SUBJECT DETAILS

Patient Samples and Primary Cell Cultures

All samples were obtained following informed consent from patients. All experimental procedures were performed in accordance with the Research Ethics Board at The Hospital for Sick Children (Toronto, Canada) and Mount Sinai Hospital (Toronto, Canada). Approval to pathological data was obtained from the respective institutional review boards. Out of 20 primary GBM samples, 6 were female and 14 were male, and ranged from 18- to 70-years of age. Three 11- to 19-week-old male human-fetal samples were a part of this study. GSC and HFNSC primary cultures were derived as previously described (Pollard et al., 2009). Briefly, samples were enzymatically and mechanically dissociated and cells were grown adherently on culture plates coated with poly-L-ornithine and laminin. Serum-free NS cell self-renewal media (NS media) consisted of Neurocult NS-A Basal media, supplemented with 2 mmol/L L-glutamine, N2 and B27 supplements, 75 μg/mL bovine serum albumin, 10 ng/mL recombinant human EGF (rhEGF), 10 ng/mL basic fibroblast growth factor (bFGF), and 2 μg/mL heparin.

Sample Nomenclature

Each sample ID follows the structure G-XXX-NS or GBM-XXX where

XXX: unique identifier of the primary sample
G-NS: glioblastoma neural stem-like cell culture
GBM: glioblastoma tissue

Animals

5- to 8-week-old NOD.Cg-Prkdc^{scid}Il2rg^{tm1Wjl}/SzJ (NSG) female mice were used for in vivo studies. All mice were subjected to stereotactic implantation of GSCs. In the DOX treatment experiment, half of transplanted mice were fed with rodent diet containing 625 mg per kg of DOX which is estimated to provide 1.6-2.7 mg of DOX daily based on a 3-5 g diet. The DOX feed was changed twice a week. Mice were age-matched in each experiment. Randomization was not performed. There were no specific inclusion or exclusion criteria. Sample sizes for experiments were determined without formal power calculations. Mice were housed at The Hospital for Sick Children Laboratory Animal Services. All experimental procedures were approved by The Hospital for Sick Children's Animal Care Committee.

Flies

Drosophila crosses were prepared in a 1:3 male to female ratio and incubated at 29°C. The parental cross was changed into a new vial after 48 hr and then again after every subsequent 24 hr for 5 days. Third instar larvae were collected on the 5th day of incubation and

CNS structures were dissected and fixed in 4% paraformaldehyde (PFA) for 20 min on ice. Dissected structures were then washed three times in 0.3% Triton-X in phosphate buffer saline (PBST) while rocking for 5 min, and stored at 4°C for up to two weeks in 0.3% PBST.

METHOD DETAILS

Transfections

Functional knockdown experiments were performed with a DN-ASCL1 construct in a PCAGGS-based backbone and an ASCL1 luciferase reporter construct (Castro et al., 2006). These constructs were introduced in GNS-ASCL1^{hi} (GliNS1, G362NS, G523NS) and GNS-ASCL1^{lo} (G377NS, G411NS) cell cultures by nucleofection with the Amaxa Nucleofector Kit. Briefly, 2 to 5 μg of DNA were transfected per 1 million cells using the program A033. After 24-48 hr post-transfection, cells were selected for GFP expression by FACS and resulted in ~40% transfection efficiencies. Plasmid encoding wild-type Cas9 was obtained from Addgene. Oligonucleotides containing target sequences were hybridized, phosphorylated, and cloned in the plasmid using BbsI sites. Target sequences of gRNAs were selected based on in silico off-target predictions from two independent sources: (1) CRISPR Design and, (2) CHOP-CHOP. GNS-ASCL1^{hi} cells (G523NS, G362NS) were transfected with each gRNA expression plasmids (2 μg each per 1 × 10^6 cells). Single cells were sorted for GFP expression 24 hr post-transfection by FACS. Single sorted GFP+ cells were sorted into 384-well plates under suspension conditions to generate clonal cultures. PCR of flanking and deleted region confirmed clones harboring heterozygous or homozygous deletions. Human ASCL1 from phASCL1-N106 was a gift from Jerry Crabtree (Yoo et al., 2011). The piggyBac transposon inducible expression PB-Tet-ON construct was a gift from Michael McGrew (Glover et al., 2013). Briefly, ASCL1 was isolated from phASCL1-N106 and subcloned into PB-Tet-ON using SmaI blunt end ligation to produce PB-Tet-ON-ASCL1. The piggyBac vector (5 μg) was co-transfected with 1 μg of piggyBac transposase Hybase per 1 × 10^6 GNS cells using nucleofection. Two days post-transfection, cells were selected with puromycin. For induced ASCL1 expression, 1 μg/mL of doxycycline hyclate was added to NS media.

Tissue and Cell Staining and Microscopy

Tissue samples were fixed for 24h with PFA, paraffin embedded and serial sectioned. Sections were deparaffinized and rehydrated through an alcohol gradient to water for antigen retrieval in 10mM citrate buffer pH 6.0 in a microwave pressure cooker. Proceeded with protocol for use of ImmPress Reagent Kit. Primary antibody was incubated overnight at 4°C. Biotinylated secondary antibody, avidin-linked peroxidase and DAB were used to detect binding of the primary antibody. Normal rabbit serum was used for control sections. Tissue sections were imaged using Nikon Eclipse Ci-L DS-FI2 and NIS-Elements Software (Nikon). Primary cell cultures were fixed for 20 min with 4% PFA and stored at 4°C for up to two weeks in PBS. Cells were blocked using 5% normal goat serum containing 0.1% Triton-X (5% NGST) for 1 hr at room temperature. Primary antibody concentration were prepared at 1:500 dilution in 5% NGST and were incubated with cells overnight at 4°C. Fluorophore-conjugated secondary antibodies were prepared at 1:500 dilution in 5% NGST and were incubated with cells for 1 hr at room temperature. Species specific isotype controls were used for control. Cells were imaged using Leica STP-6000 microscope. Fly tissues were blocked using 5% normal goat serum in 0.3% PBST for 1 hr at room temperature. 10-15 *Drosophila* CNS structures were used for each primary antibody staining condition which were prepared at the following concentrations in blocking solution: 2.5 μg/mL mouse anti-Cyclin B, 1 μg/mL rat anti-Elav, and 0.68 μg/mL mouse anti-repo. CNS structures were incubated in 100uL of primary antibody for 1 hr at room temperature and then washed 3 times for 5 min while rocking in 0.3% PBST. Secondary antibodies of goat anti-primary antibody species (rabbit, mouse and rat) were prepared at a concentration of 4 μg/mL in blocking solution and CNS structures were incubated for 2 hr at room temperature. 3 washes for 5 min each in 0.3% PBST were then performed and CNS structures were either cleaned and mounted immediately or kept over-night at 4°C and cleaned and mounted the following day. To clean the structures, as much non-CNS tissue as possible was removed. To mount, structures were placed on glass coverslips in Vectashield H-1200 fluorescent mounting medium containing Dapi. A glass slide was gently placed on top of the CNS structures and stuck to the coverslip with wax. Coverslips with stained structures were kept at 4°C until they were imaged using a Leica SP8 Confocal microscope.

In Vitro Differentiation Assay

Differentiation experiments were performed by sequential withdrawal of rhEGF and bFGF, as previously described (Pollard et al., 2009). Cells were seeded in NS media. After 1-2 days under self-renewing conditions, media was changed to NS media containing reduced bFGF (5 ng/mL) and without rhEGF. After 7 days, media was changed to Neurobasal media containing without rhEGF and bFGF, and cells were cultured under these conditions for an additional 14 days. Neuronal differentiation experiments were performed by culturing cells in NS media containing 5 μM of L-685,458 in dimethyl sulfoxide (DMSO) for 14 days. Media was changed every 2 days.

In Vitro Cell Proliferation Assay

Cells were plated adherently in biological triplicates on a 24-well plate. Cells were incubated with Accutase for 5 min at 37°C. Absolute number of live cells were detected using Trypan Blue dye exclusion assay. Cells were quantified over 8 – 16 days and population doubling times were calculated using data collected at 2 time-points during logarithmic growth phase. EdU was added to cell cultures at a concentration of 10 μM and incubated for 3 hr prior to cell fixation.

In Vitro Limiting Dilution Assay

Cells were plated in serial dilutions on non-adherent 96-well plates and in six biological replicates under NS conditions. Serial dilutions ranged from 2000 cells to 3 cells per well. After 7 and 14 days of plating, each well was scored for negative spheres. Data was plotted and tested for inequality in frequency between multiple groups and tested for adequacy of the single-hit model using Extreme Limiting Dilution Analysis (ELDA) software.

In Vitro Live-Cell Imaging

Cells were plated adherently in 12 biological replicates on a 24-well plate and imaged using IncuCyte ZOOM. Cells were imaged using phase-contrast every 4 hr over 10 days. Cell confluency and neurite branch measurements were made using IncuCyte live cell analysis system and NeuroTrack processing software.

In Vivo Transplantation Assay and Treatment

NSG female mice were anaesthetized using gaseous isoflurane and immobilized in a stereotaxic head frame. An incision was made at the midline and bore-hole drilled using a 21G needle 1 mm lateral and 2 mm posterior to bregma. Cells were injected 2.5 mm deep to the surface of the skull using a Hamilton syringe and 27 G needle over a period of 3 min. To avoid reflux, the needle was left in place for 4 min after injection and gradually withdrawn over 3 min. The bore-hole was then filled with bone wax and incision closed with 5.0 sutures. Mice were observed for signs of tumor formation or sacrificed after 6 months of follow-up.

In Vivo Secondary Transplantation Assay

Mice displaying signs of morbidity were sacrificed and whole brains containing xenograft tumors were harvested. Tissues were dissociated into single-cell suspensions by a combination of mechanical and enzymatic dissociation. Mouse cells were depleted from cell suspensions using the Mouse Cell Depletion Kit. Isolated human tumor cells were counted and 10-fold dilutions of 20,000 and 2,000 GSCs were re-transplanted for each treatment group.

Experimental Design

One of the main goals of this project was to study the variability in the molecular status of ASCL1 and the drug response to GSI. Thus, different levels of replication were used: tumor biological replicates (where different patient samples for drug responsiveness and ASCL1 functional studies), biological replicates of individual tumor sample (where cell activity assays were repeated at least twice for each independent GSC culture), biological replicates in cell activity assays (where independent cultures of the same GSC culture were quantified at least three times), and technical replicates for in vivo studies (where 3 independent tumor engraftments were re-engrafted into 4 mice during the secondary transplantation). No specific strategy for randomization was employed, and no blinding was used, except for in vivo validations of tumor morbidity.

RNA Sequencing Analysis

Cells were cultured adherently for 7 days. Total RNA was extracted using RNeasy Mini Kit and treated with DNase. RNA was measured for quality using Bioanalyzer (Agilent) and RNA-seq libraries (3 replicates each for $ASCL1^{WT}$ Vehicle, $ASCL1^{WT}$ GSI, $ASCL1^{KO}$ Vehicle, $ASCL1^{KO}$ GSI, $ASCL1^{KO}$ Untreated, $ASCL1^{KO}$ DOX), enriched for stranded poly(A) mRNA, and sequenced on Illumina HiSeq 2500 (Illumina). The starting number of read pairs was approximately 40 million per sample (100 bp paired-end), ~85% of which were retained after trimming low quality regions and adaptor sequences. The raw trimmed reads were aligned to the reference genome (UCSC hg19). Two-condition differential expression was done with the edgeR R package, v.3.8.6. Pathway and gene ontology analyses were performed using GSEA and ranked differential gene expression and the Bader lab gene set (Human_GO_AllPathways_no_GO_iea_September_24_2015_symbol.gmt). GSEA results were visualized in Cytoscape v.3.3.0 using the Enrichment Map application.

ChIP Sequencing Analysis

Cells were untreated or treated with 1 μg/mL doxycycline for 18 hr (12×10^6 cells per replicate; n = 3 replicates total for each condition). Cells were fixed using 11% formaldehyde and sonicated using a focused-ultrasonicator (Covaris) for 20 min resulting in 200 μg of soluble chromatin in total. Lysates were clarified from sonicated nuclei and ASCL1-DNA complexes were isolated from 40 μg of chromatin and 5 μg of ASCL1 antibody (BD PharMingen Lot#5121666), rocking overnight at 4°C. Library was validated by Bioanalzyer and Kapa qPCR assay and sequenced on an Illumina HiSeq 2500 platform, using a Rapid Run mode flowcell to generate paired end reads of 100 bases. ChIP-seq reads were aligned to the hg19 genome using bowtie2 and trimmed to positions 6-65. Alignments were filtered to keep only reads mapping in a concordant pair. Reads were further filtered for duplicates, unmapped contigs, random contigs, overlaps with the ENCODE blacklist, and low quality mappings. Replicates were merged before peak calling. ASCL1-bound regions were detected using MACS2 v2.0.10 with default settings and a q-value filter of 0.05. Peaks were annotated as promoter peaks if they overlapped with a 3kb window around a Gencode v19 transcription start site (2.5kb upstream, 0.5 kb downstream). Overlaps between open chromatin and ASCL1 binding sites were determined using bedtools v2.23. Those peaks that were not annotated to promoters and did not overlap open chromatin regions were linked to their target genes with C3D; in this case, the list of 'new' ASCL1 binding sites was added to the list of open regions as determined by ATAC-seq and this full list was used as the set of open regions in C3D.

ATAC Sequencing Analysis

ATAC-seq was used to profile the open chromatin landscape of 11 GNS lines as previously described (Buenrostro et al., 2013). Briefly, cryopreserved (10% DMSO) cell suspensions were quickly thawed at 37°C, and resuspended in 10 mL by dropwise addition of warm PBS. Cells were then spun at 600xg for 10min, resuspended in 1mL PBS and 50,000 live cells were counted out with a trypan blue stain. After spinning the cells down at 600xg for 10min, they were resuspended in lysis buffer (10mM Tris-HCl pH 7.4, 10mM NaCl, 3mM MgCl2, 0.1% IGEPAL CA-630) and kept on ice for 5 min. The cells were then spun down a final time at 600xg for 10min, resuspended in 50ul of transposase mix (Illumina Nextera DNA Sample Preparation Kit), and incubated at 37°C for 30min. After clean-up with QIAGEN MinElute, the open chromatin regions were amplified by PCR. The resulting libraries were sequenced with 50 bp single-end reads which were mapped to hg19. Reads were filtered to remove duplicates, unmapped or poor quality ($Q < 30$) reads, mitochondrial reads, chrY reads, and those overlapping the ENCODE blacklist. Following alignment, open chromatin regions/peaks were called using MACS2. Default parameters were used except for the following:–keep-dup all -B–nomodel–SPMR -q 0.05–slocal 6250–llocal 6250. The signal intensity was calculated as the fold enrichment of the signal per million reads in a sample over a modeled local background using the bdgcmp function in MACS2. The distribution of genomic features across the ATAC peaks was determined using CEAS (Shin et al., 2009). Interactions between regions of open chromatin were predicted using Cross-cell-type correlation in DNase I hypersensitivity (C3D).

Motif Enrichment Analysis

ASCL1-bound genomic regions were tested with homer v4.7 (Heinz et al., 2010) to detect enrichments of transcription factor binding motifs.

QUANTIFICATION AND STATISTICAL ANALYSIS

Statistical analysis of differential ASCL1 expression was performed in GraphPad Prism and significance was calculated with the Mann Whitney test (Figure 1A). Statistical analysis for differential gene expression of exon microarray data were performed in R and significance was calculated with Student's t test (Figure 1G). Statistical analysis of qPCR data was performed in GraphPad Prism and significance was calculated with One-way ANOVA. Values were obtained from 2 biological replicates and 2-3 technical replicates for each sample and were normalized to ACTB and/or GAPDH. Data is presented as median ± SD (Figures 1F, 1H, and S1A) mean ± SD (Figures S1L–S1N, S2P, and 3B). Statistical analysis of immunocytochemical data was performed in GraphPad Prism and significance was calculated using an unpaired t test corrected for multiple comparisons using the Holm-Sidak method. Error bars, mean ± SEM (2-4 biological replicates and 4 technical replicates; Figures 1E, 2B, 2C, 2H, 2K, 2L, 3F, 3K, 5D, S1D, S1G, S1P, S2D–S2G, S3C, S3D, and S3F). For fly immunohistochemical data, statistical analysis was performed in GraphPad Prism and significance was calculated unpaired two-tailed t test. Error bars represent mean ± SD (n = 8-22 biological replicates; Figures 4E–4I). Live-cell imaging analysis was plotted using GraphPad Prism. Error bars represent mean ± SD (n = 12 biological replicates; Figures 3D and S1Q). In vitro limiting dilution analysis was performed in ELDA and SFC is plotted as 95% confidence intervals for 1/(stem cell frequency). Pairwise chi-square tests were used to test for differences in stem cell frequencies between treatment groups (Figures 1I–1L, 2I, 3H, 3I, 3L, S1H–S1J, S2J–S2M, and S4C). Survival was measured according to the Kaplan-Meier method. Log-rank (Mantel-Cox) test was used to compare survival curves. The sample size for each experiment, n, is included in the results section and the associated figure legend (Figures 1B, 2G, 2H, 4B, 4C, S1B, and S1C). Statistical analysis of proliferation was performed in GraphPad Prism and significance was calculated using Two-way ANOVA test to compare means between each group. Error bars, mean ± SEM (n = 3 biological replicates; Figures 2D, S2H, and S2I). In all figures: *, $p < 0.05$; **, $p < 0.01$; ***, $p < 0.001$; ****, $p < 0.000$.

Details and Number of Samples Analyzed

Exon-Microarray

Number of different samples sequenced: 4
HF240NS, HF5205NS, G179NS, G144NS
Number of different models: 3
Time points 0, 2, and 9 days of the in vitro differentiation protocol.

RNA-Sequencing

Number of different samples sequenced: 2
G523NS-ASCL1^{WT}, G523NS-ASCL1^{KO}
Number of different models: 4 (n = 3 biological replicates)
GSI treatment, vehicle treatment, doxycycline treatment, naive treatment.

ChIP-Sequencing

Number of different samples sequenced: 1
G523NS-ASCL1^{KO}
Number of different models: 2 (n = 3 biological replicates)
Doxycycline treatment, naive treatment

ATAC-Sequencing

Number of different samples sequenced: 12
G489NS, G799NS, G754NS, G719NS, G549NS, G705NS, G411NS, G702NS, G571NS, G729NS, G797NS, G523NS-ASCL1^{KO}
Number of different models: 2 (n = 2 biological replicates)
Doxycycline treatment, naive treatment

DATA AND SOFTWARE AVAILABILITY

The accession number for the exon microarray data reported in this paper is GEO: GSE87619. The accession numbers for the RNA-seq data reported in this paper are GEO: GSE87617 and GEO: GSE87615. The accession number for the ChIP-seq data reported in this paper is GEO: GSE87618. The accession number for the ATAC-seq data reported in this paper is GEO: GSE96088.